

1 **Reply to the Interactive comment of Anonymous Referee #1 on “Processes controlling the**
2 **seasonal variations of ^{210}Pb and ^7Be at the Mt. Cimone WMO-GAW global station, Italy:**
3 **A model analysis” by Erika Brattich et al.**

4
5 Manuscript Ref: acp-2016-568

6
7 We thank Reviewer # 1 for the detailed comments on our manuscript. Below please find our
8 itemized replies.

9
10 1) *page 10, line 9: What is the spatial resolution of the model simulations?*

11 Reply – We have added this information in the text: “Meteorological data used to drive the
12 CTM at 2° latitude by 2.5° longitude resolution, e.g., horizontal winds, convective mass fluxes
13 and precipitation fields, are the Modern-Era Retrospective analysis for Research and
14 Applications (MERRA) assimilated data set from the NASA Global Modeling and
15 Assimilation Office (GMAO) (Rienecker et al., 2011).”

16
17 2) *page 11, lines 3-6: The authors state " For the simulations of radionuclides, each*
18 *simulation was run for six years, recycling the meteorological data for each year of the*
19 *simulation, to equilibrate the lower stratosphere as well as the troposphere". Does this*
20 *practically mean that it is simulated the same year for six times and that the first five years*
21 *were used as a spin up time? Also please mention again here that the actual year of the*
22 *simulation is 2005.*

23 Reply – Yes. Thanks for pointing it out. Now the text reads “For the simulations of
24 radionuclides, each simulation was run for six years, recycling the MERRA meteorological

1 data for 2005, to equilibrate the lower stratosphere as well as the troposphere (Liu et al., 2001).
2 The sixth-year output was used for analysis.”

3

4 3) *page 13, lines 20-21: The authors state that " In the model Mt. Cimone appears to be*
5 *in a location where there is a large horizontal gradient of wind (transport)." Mind though that*
6 *the model's winds in Figure 2 are from specific months in a single year (the year 2005) and*
7 *hence do not actually represent a wind climatology of the respective months.*

8 Reply – Indeed, the model's winds in Figure 2 are from specific months in a single year (2005)
9 and do not represent a wind climatology of the respective months. However, we do not mean
10 to represent a wind climatology here. We have revised the sentence to “In the model Mt.
11 Cimone appears to be in a location where there is a large horizontal gradient of wind (transport)
12 during 2005.”

13

14 4) *page 14, line 10-14: Note also that the etesian wind system at eastern Mediterranean*
15 *in July is also well represented in Figure 2.*

16 Reply – Indeed. We have added a sentence at the end of this paragraph: “However, MERRA is
17 able to capture the summertime north-north easterly winds in the eastern Mediterranean
18 (Aegean Sea), known as the Etesian winds, generated by thermal effects.”

19

20 5) *page 15, line 11-14: The authors state that "Large differences between the MERRA*
21 *precipitation and that locally observed at the station are instead present (not shown): in*
22 *particular, the MERRA precipitation is larger during winter-autumn, while it is much more*
23 *similar to that observed during spring-summer." I would suggest to add information or a graph*
24 *with the station-based observations of precipitation at Mt Cimone (even as supplementary*
25 *material). Of course, MERRA data reflect large scale precipitation features while the station-*

1 *based observations reflect local features. Nevertheless in your analysis you compare modelled*
2 *Pb-210 and Be-7 radionuclide concentrations with the respective station based measurements*
3 *at Mt Cimone, but these station based radionuclide measurements are presumably linked more*
4 *with the local observation of precipitation than with large scale MERRA precipitation data.*

5 Reply - We thank the reviewer for the suggestion. As reported later on in the manuscript (page
6 15, lines 16-22) the local precipitation pattern at Mt. Cimone is different from the regional
7 pattern of the surrounding area, and this difference could partially explain the disagreement
8 between the observed and simulated pattern of precipitation. As commented by the reviewer
9 and discussed in the paper (page 14, lines 23-25; page 15, lines 1-2), local precipitation at the
10 site is important to the scavenging of radionuclides and the difference between the observed
11 and MERRA precipitation could contribute to the biases in our model simulations due to the
12 errors in the precipitation scavenging of radionuclides. We have added information and revised
13 the text to "Large differences between the MERRA precipitation and that locally observed at
14 the station are instead present. While the daily mean observed 2005 precipitation is 0.81 mm,
15 which is close to the corresponding precipitation (0.73 mm) in MERRA at the "ij" grid (i.e., a
16 negative bias of -0.08 mm); the model bias is positive and much higher (0.31 – 1.28 mm) at
17 adjacent grids. This bias may very well reflect again the fact that the observed surface
18 precipitation is localized, whereas the satellite and MERRA precipitations correspond to a
19 much larger scale (about 200 km)."

20

21 6) *page 17, line 21-23: The authors state that "The correlation between observed and*
22 *simulated monthly ⁷Be activities also increases from $R^2 = 0.03$ at "ij" to $R^2 = 0.11-0.60$ at*
23 *adjacent model gridboxes." Please specify at which grid-box you get 0.6 and discuss the reason*
24 *for this considerable improvement.*

1 Reply – The revised text reads “The largest value of $R^2 = 0.6$ was obtained at the “ij-1” gridbox
2 to the south of “ij” (Figure 6). This improvement is due to the large horizontal gradient in the
3 simulated ^7Be concentrations near the site (Figure 2).”

4

5 7) *page 17, line 21-23: The authors state that " As for ^7Be , the model well captures the*
6 *March maximum (i.e., secondary maximum in the observations) and the general seasonal*
7 *pattern during the cold and transition seasons." I think that this statement is not very consistent*
8 *with Figure 5b. Actually, according to Figure 5b the model does not seem to capture the*
9 *general seasonal pattern for Be-7.*

10 Reply – To avoid confusion, we have revised the sentence to “As for ^7Be , the model well
11 captures the March maximum (i.e., secondary maximum in the observations) and the month-
12 to-month variation during the cold and transition seasons (January-April, October-December).”

13

14 8) *page 18, line 19-21: The authors state that " The simulated seasonal pattern of the*
15 *$^{10}\text{Be}/^7\text{Be}$ ratio is very similar to the observations at Zugspitze (Germany, 2962 m asl) (Zanis et*
16 *al., 2003), characterized by a not-pronounced seasonal cycle". In fact the simulated Be-10/Be-*
17 *7 ratio in Figure 5d has a clear seasonal cycle and looking the respective graph Figure 3 from*
18 *the cited paper of Zanis et al., 2003, I see a better agreement with Jungfraujoch than with*
19 *Zugspitze.*

20 Reply - Thanks the reviewer for pointing this out to us. Accordingly, we have revised the text
21 to “The simulated seasonal pattern of the $^{10}\text{Be}/^7\text{Be}$ ratio is very similar to the observations at
22 Jungfraujoch (Switzerland, 3580 m asl) (Zanis et al., 2003), characterized by a clear seasonal
23 cycle with peak ratios in spring.”

24

1 9) page 19, line 9-11: The authors state that " However, the model tends to overestimate
2 the observed ^7Be concentrations and $^7\text{Be}/^{210}\text{Pb}$ ratios during December-February, suggesting
3 that STE and/or subsidence in the model is likely too fast in this region." This is a rather
4 speculative comment. It needs more justification. What do you mean with too fast? Maybe
5 stronger STE fluxes? Are there any references showing how the STE fluxes of this model
6 compares with other global CTMS or GCMs?

7 Reply – This statement is for the site of Mt. Cimone and year 2005, and is only suggestive. To
8 address the reviewer's concern, we have added a new reference and revised the text to
9 "However, the model tends to overestimate the observed ^7Be concentrations and $^7\text{Be}/^{210}\text{Pb}$
10 ratios during December-February, suggesting that stratospheric influence and/or subsidence in
11 the model is probably too strong in this region at this time of the year. It is noted that globally
12 integrated STT mass fluxes in the MERRA reanalysis are actually smaller than in some other
13 reanalyses, e.g., ERA-Interim, JRA-55, and MERRA-2 (Boothe and Homeyer, 2016)."

14
15 10) page 19, line 11-13: The authors state that "As reported by Huang et al. (2013), a
16 stronger net subsidence of air masses to the surface could be due to unrealistic meteorological
17 conditions (e.g., boundary layer structure, wind fields, vertical mixing)." This is a rather
18 general comment. Is this true for the meteorological data used here in the CTM? Please clarify
19 this issue.

20 Reply – To avoid confusion, we have removed this sentence.

21
22 11) page 20, line 19-20: The authors state that "The model annual average biases are about
23 8% for ^{210}Pb and about 19% for ^7Be , respectively. By contrast, the model average bias for
24 $^7\text{Be}/^{210}\text{Pb}$ ratios is about -13% (Figure 7)." Please comment on the error propagation on the
25 ratio.

1 Reply – We comment on the error propagation on the ratio after this statement: “The smaller
2 model bias for ${}^7\text{Be}/{}^{210}\text{Pb}$ ratios than for ${}^7\text{Be}$ concentrations reflects the fact that the ratio cancels
3 out the errors in precipitation scavenging (Koch et al. 1996) that contribute to the underestimate
4 of ${}^{210}\text{Pb}$ and ${}^7\text{Be}$ activities. On the other hand, the negative model bias for the ${}^7\text{Be}/{}^{210}\text{Pb}$ ratio
5 again points to weak downward mixing from the free troposphere.”

6
7 12) page 22, line 8-9: *The authors state that " ... suggesting that large-scale circulation in
8 this region with complex topography may not be resolved by the coarse-resolution model." I
9 guess you mean that regional and local circulations are not resolved by the global model.*

10 Reply – Indeed. We have revised the sentence to “None of our simulations is able to describe
11 the observed ${}^7\text{Be}$ summertime peak, suggesting that local and regional circulations in this
12 region with complex topography may not be resolved by the coarse-resolution model.”

13
14 13) page 24, line 1-4: *The authors state that "The model underestimate of ${}^7\text{Be}$ levels in the
15 warm months is partly due to the sensitivity to spatial sampling in the model, but also suggests
16 that the mixing of air masses between the PBL and the lower free troposphere is likely too
17 weak." If the model mixing between the PBL and the lower free troposphere becomes stronger
18 then this will result in more mixing of PBL air poor in Be-7 with free tropospheric air, hence
19 even smaller concentrations of Be-7 and larger model underestimate of Be-7 at Mt Cimone.*

20 Reply - The vertical mixing between the PBL and the lower free troposphere includes both an
21 upward motion from the PBL to the lower free troposphere (poor in ${}^7\text{Be}$), and a downward
22 motion from the lower free troposphere to the PBL (richer in ${}^7\text{Be}$). We have changed the
23 sentence to “The model underestimate of ${}^7\text{Be}$ levels in the warm months is partly due to the
24 sensitivity to spatial sampling in the model, but also suggests that the mixing of air masses
25 between the PBL and the lower free troposphere (e.g., via convection and compensating

1 subsidence) is likely too weak during summer when the Mt. Cimone station is located within
2 the PBL.”

3
4 *14) To my understanding, the authors claim that the CTM cannot capture the observed*
5 *seasonal cycle of Be-7 with a summer max at Mt Cimone because of local features which are*
6 *not resolved in the model. However mind that the summer maximum Be-7 at Mt Cimone is also*
7 *apparent at Jungfraujoch, Sonnblick and Zugspitze (see e.g. Figure 7 in Gerasopoulos et al.,*
8 *2001). So maybe this feature does not seem to be a very local phenomenon but is rather of*
9 *larger horizontal scale.*

10 Reply - The fact that the CTM cannot capture the observed seasonal cycle of ⁷Be is due to a
11 combination of factors. Firstly, results show sensitivity to spatial sampling in the model, which
12 can be clearly seen from a better simulated ⁷Be seasonal cycle at some adjacent gridboxes.
13 Secondly, the summer ⁷Be maximum observed at mountain sites such as Mt. Cimone,
14 Jungfraujoch, Sonnblick, and Zugspitze results from downward transport of ⁷Be due to
15 compensating subsidence associated with summertime convective mixing (Gerasopoulos et al.,
16 2001), which the coarse-resolution model may not be able to correctly represent.

17

18

19

20

21

22

23

1 **Reply to the Interactive comment of Anonymous Referee #2 on “Processes controlling the**
2 **seasonal variations of ^{210}Pb and ^7Be at the Mt. Cimone WMO-GAW global station, Italy:**
3 **A model analysis” by Erika Brattich et al.**

4
5 Manuscript Ref: acp-2016-568

6
7 We thank reviewer # 2 for helpful comments. Below please find our itemized replies.

8
9 *1) How about the actual precipitation at Mt. Cimone in Figure 4? The difference between*
10 *actual, modeled, and GPCP precipitations would support that wet scavenging is the main*
11 *reason controlling ^7Be seasonal variations shown in Figure 8. Please notice the precipitation*
12 *comparisons in Figure 4 (ij), which shows that the model precipitation is generally lower than*
13 *that of GPCP, meaning that the modeled wet scavenging processes perhaps is lower than the*
14 *reality. This weak modeled wet scavenging seems to be very significant for the ^7Be*
15 *concentrations shown in Figure 8.*

16 Reply – We thank the reviewer for pointing this out. We have revised the text as follows: “The
17 MERRA precipitation is generally lower than that of GPCP at two gridboxes (except for
18 summer, Figure 4ab), but in good agreement at the other two gridboxes (Figure 4cd). Large
19 differences between the MERRA precipitation and that locally observed at the station are
20 instead present. While the daily mean observed 2005 precipitation is 0.81 mm, which is close
21 to the corresponding precipitation (0.73 mm) in MERRA at the “ij” grid (i.e., a negative bias
22 of -0.08 mm); the model bias is positive and much higher (0.31 – 1.28 mm) at adjacent grids.
23 This bias may very well reflect again the fact that the observed surface precipitation is
24 localized, whereas the satellite and MERRA precipitations correspond to a much larger scale
25 (about 200 km).”

1
2 2) One section can be added to illustrate the model results of this study in comparison with
3 historical model studies. Those model studies may include as follows: ^7Be : Brost, et al., *J*
4 *Geophys Res*, 96, 1991; ^{210}Pb : Feichter, et al., *J. Geophys. Res.*, 96, 1991; Lee, H. N., et al., *J*
5 *Geophys. Res.*, 109, D22203, 2004, doi: 10.1029/2004JD005061. $^7\text{Be}/^{210}\text{Pb}$: Koch et al., *J*
6 *Geophys. Res*, 101(D13), 1996.

7 Reply – Thanks for the suggestion. Since our focus is on the model analysis of observational
8 data from a single station (versus global simulations of ^{210}Pb , ^7Be , and $^7\text{Be}/^{210}\text{Pb}$), we have
9 decided to cite these historical model studies in various places of the text.

10
11 3) The WMO-GAW station, Mt. Cimone (44°12' N, 10°42' E, 2165 m asl, Italy) is quite close
12 to the Alps stations, such as Jungfraujoch (46.32°N, 7.59°E, elevation 3580 m asl) and
13 Zugspitze (47. °N, 11.0°E, 2962 m a.s.l.) in the model grids. How about the general results of
14 the model and observation comparisons for those two stations in 2005? I believe these
15 comparisons will support the conclusion that coarse of the model runs is one of the reasons for
16 the worse ^7Be comparisons.

17 Reply – Unfortunately, we cannot compare the results of our simulations with the observations
18 from Jungfraujoch and Zugspitze stations in 2005. We own only the Mt. Cimone data, and the
19 observational data from other stations are not publicly available.

20
21 4) For Figure 8, I am confused that without the wet-scavenging process, the ^{210}Pb
22 concentration is even lower than that of observed from January to July. The convection uplift
23 of ^{222}Rn seems does not support the summer ^{210}Pb maximum but on the contradictory. How
24 about the sensitivity experiments with case of $^7\text{Be}/^{210}\text{Pb}$ in Figure 8? Why do you show the
25 sensitivity test for $ji-1$ grid rather than the ji grid in this figure?

1 Reply - The model result without scavenging is not lower than that observed from January to
2 July. Since the simulation without wet scavenging resulted in concentrations far higher than
3 those obtained in the standard simulation and in other sensitivity experiments, the results from
4 that simulation are plotted on a different scale (see the right y-axis of Figure 8). As discussed
5 in the manuscript, the model simulation without convection results in larger ^{210}Pb
6 concentrations in the free troposphere due to the compensating effects of convective transport
7 and scavenging. We have not reported the $^7\text{Be}/^{210}\text{Pb}$ ratios from sensitivity experiments since
8 the ratio is not affected by scavenging. We have chosen to show the sensitivity tests for grid
9 “ij-1” rather than “ij”, since at the former a better comparison between the observed and
10 simulated ^{210}Pb and especially ^7Be activities was found. Also see Figures 5-6 and their
11 discussions.

12

13

14

15

16

17

18

19

20

21

22

1 **Reply to the Interactive comment of Editor J. Ma on “Processes controlling the seasonal**
2 **variations of ^{210}Pb and ^7Be at the Mt. Cimone WMO-GAW global station, Italy: A model**
3 **analysis” by Erika Brattich et al.**

4
5 Manuscript Ref: acp-2016-568

6
7 We thank the editor for his comments. Below please find our itemized responses.

8
9 *1). The authors may consider giving a brief description of what the physical and chemical*
10 *processes are included in their model for the simulation of radionuclides Pb-210 and Be-7 in*
11 *both the stratosphere and the troposphere, instead of just referring to the literatures (Page 10,*
12 *Line 9-14).*

13 Reply - We thank the editor for his comment. A brief description of the physical and chemical
14 processes included in the GMI model used for the simulation of ^{210}Pb and ^7Be radionuclides in
15 the stratosphere and the troposphere is given as follows. “In this work, we simulate ^{222}Rn , ^{210}Pb ,
16 ^7Be , and ^{10}Be using a version of the GMI model with the same basic structure as described by
17 Considine et al. (2005) and Liu et al. (2016), including parameterizations of the important
18 tropospheric physical processes such as convection, wet scavenging, dry deposition and
19 planetary boundary layer mixing. Meteorological data used to drive the CTM at 2° latitude by
20 2.5° longitude resolution, e.g., horizontal winds, convective mass fluxes and precipitation
21 fields, are the Modern-Era Retrospective analysis for Research and Applications (MERRA)
22 assimilated data set from the NASA Global Modeling and Assimilation Office (GMAO)
23 (Rienecker et al., 2011).” “The flux-form semi-Lagrangian advection scheme and a convective
24 transport algorithm from the CONVTRAN routine in NCAR CCM3 physics package are used
25 in the model. The wet deposition scheme is that of Liu et al. (2001): it includes scavenging in

1 wet convective updrafts, and first-order rainout and washout from both convective anvils and
2 large-scale precipitations. The gravitational settling effect of cloud ice particles included in Liu
3 et al. (2001) is not considered here. Dry deposition of aerosols is computed using the resistance-
4 in-series approach.”

5
6 2). *Pb-210 and Be-7 were analyzed from the PM10 samples according to a description of the*
7 *radionuclide measurement (Page 9, Line 5-8). I wonder if the treatment of aerosol processes*
8 *in the model could affect the simulation of radionuclides. How does the model treat the uptake*
9 *of radionuclides on particulate matters? Does the uncertainties in the simulation of PM10*
10 *affect the simulation results of Pb-210 and, in particular, Be-7?*

11 Reply – The model does not specifically simulate aerosols particles to which the radionuclides
12 attach. Instead, those aerosol particles are assumed to be ubiquitous. Now we state in
13 Introduction: “Once produced, both radionuclides rapidly attach to ubiquitous submicron
14 aerosol particles in the ambient air (Papastefanou and Ioannidou, 1995; Winkler et al., 1998;
15 Gaffney et al., 2004; Ioannidou et al., 2005), and are removed from the atmosphere mainly by
16 wet and secondarily dry deposition (Kulan et al., 2006).”

17
18 3). *The treatment of Be-7 source in the model is also suggested to be described more*
19 *specifically, e.g., by providing the prescribed concentrations or by giving the production rates*
20 *at certain altitudes.*

21 Reply – We have added more information on the ⁷Be source in the model: “Following Brost et
22 al. (1991) and Koch et al. (1996), we used the Lal and Peters (1967) ⁷Be source for 1958 (solar
23 maximum year), as it best simulated stratospheric ⁷Be concentrations measured from aircraft
24 (Liu et al., 2001). The rates of ⁷Be production reported more recently by Usoskin and Kovaltsov
25 (2008) broadly agree with those of Lal and Peters (1967) with slightly (about 25%) lower global

1 production rate and will be tested in a separate model study. The Lal and Peters (1967) source
2 is represented as a function of latitude and altitude (pressure) and does not vary with season
3 (see Figure 1 of Koch et al., 1996).”

4

5

6

7

8

9

10

11

12

13

14

15

16

17

18

19

20

1 Processes controlling the seasonal variations of ^{210}Pb and ^7Be
2 at the Mt. Cimone WMO-GAW global station, Italy: A model
3 analysis

4 Erika Brattich¹, Hongyu Liu², Laura Tositti¹, David B. Considine³, and James H. Crawford⁴

5 [1] Department of Chemistry “G Ciamician”, Alma Mater Studiorum University of
6 Bologna, Bologna (BO), 40126, Italy

7 [2] National Institute of Aerospace, Hampton, Virginia, Virginia, VA 23681, USA

8 [3] NASA Headquarters, Washington, DC 20546, USA

9 [4] NASA Langley Research Center, Hampton, Virginia, VA 23681, USA

10

11 **Correspondence to:** Hongyu Liu (hongyu.liu-1@nasa.gov)

12 **Abstract.** We apply the Global Modeling Initiative (GMI) chemistry and transport model
13 driven by the NASA’s MERRA assimilated meteorological data to simulate the seasonal
14 variations of two radionuclide aerosol tracers (terrigenous ^{210}Pb and cosmogenic ^7Be) at the
15 WMO-GAW station of Mt. Cimone (44°12’ N, 10°42’ E, 2165 m asl, Italy), which is
16 representative of free-tropospheric conditions most of the year, during 2005 with an aim to
17 understand the roles of transport and precipitation scavenging processes in controlling their
18 seasonality. The total precipitation field in the MERRA data set is evaluated with the Global
19 Precipitation Climatology project (GPCP) observations, and a generally good agreement is
20 found. The model reproduces reasonably the observed seasonal pattern of ^{210}Pb concentrations,
21 characterized by a wintertime minimum due to lower ^{222}Rn emissions and weaker uplift from
22 the boundary layer and summertime maxima resulting from strong convection over the

1 continent. The observed seasonal behavior of ^7Be concentrations shows a winter minimum, a
2 summer maximum, and a secondary spring maximum. The model captures the observed ^7Be
3 pattern in winter-spring, which is linked to the larger stratospheric influence during spring.
4 However, the model tends to underestimate the observed ^7Be concentrations in summer,
5 partially due to the sensitivity to spatial sampling in the model. Model sensitivity experiments
6 indicate a dominant role of precipitation scavenging (versus dry deposition and convection) in
7 controlling the seasonality of ^{210}Pb and ^7Be concentrations at Mt. Cimone.

8

9 **1 Introduction**

10 The use of atmospheric radionuclides to understand atmospheric dynamics, pollution
11 transport and removal processes has a long history (e.g., Junge, 1963; Reiter et al., 1971;
12 Gägeler, 1995; Arimoto et al., 1999; Turekian and Graustein, 2003; WMO-GAW, 2004; Dibb,
13 2007; Rastogi and Sarin, 2008; Froehlich and Masarik, 2010; Lozano et al., 2012). It has been
14 recognized that natural radionuclides are useful in a global monitoring network for atmospheric
15 composition to support global climate change and air quality research, and therefore they are
16 measured at many of the regional, global and contributing-partner stations in the Global
17 Atmosphere Watch (GAW) network of the World Meteorological Organization (WMO)
18 (WMO-GAW, 2004). In particular, terrigenous ^{210}Pb and cosmogenic ^7Be natural radionuclides
19 are helpful in the understanding of the roles of transport and/or scavenging in controlling the
20 behaviors of radiatively active trace gases and aerosols ([Feichter et al., 1991](#); Balkanski et al.,
21 1993; Koch et al., 1996), as well as their anthropogenic (vs. natural) origin (e.g., Graustein and
22 Turekian, 1996; Arimoto et al., 1999; Liu et al., 2004; Cuevas et al., 2013). They are routinely
23 monitored at WMO-GAW stations around the world (Lee et al., 2004). Although ^{210}Pb and ^7Be
24 have long (1998-2011) been measured at the Global WMO-GAW station of Mt. Cimone (Italy),
25 their seasonal behavior has not been thoroughly elucidated (Lee et al., 2007; Tositti et al.,

1 2014). Here we apply a state-of-the-art global chemistry and transport model (CTM) to the
2 simulation of ^{210}Pb and ^7Be , with an objective to better understand the roles of transport and
3 precipitation scavenging processes in controlling their seasonal variations at Mt. Cimone.

4 Because of their contrasting natural origins, ^{210}Pb and ^7Be have been used as a pair to
5 study the vertical transport and scavenging of aerosols (Koch et al., 1996). ^{210}Pb (half-life $\tau_{1/2}$
6 = 22.3 years) is the decay daughter of ^{222}Rn ($\tau_{1/2} = 3.8$ days), which is emitted from soils by
7 decay of ^{226}Ra . The oceanic input of ^{222}Rn is about two orders of magnitude less than the
8 continental input and, because of the continental origin of ^{222}Rn , ^{210}Pb is considered as a tracer
9 of air masses with continental origin (Baskaran, 2011). ^7Be ($\tau_{1/2} = 53.3$ days) is a cosmogenic
10 radionuclide generated by cosmic ray spallation reactions with nitrogen and oxygen (Lal et al.,
11 1958). Most (~67%) of ^7Be is produced in the stratosphere and the remaining (~33%) is
12 generated in the troposphere, particularly in the upper troposphere (Johnson and Viezee, 1981;
13 Usoskin and Kovaltsov, 2008). ^7Be is thus considered a tracer of stratospheric influence
14 (Viezee and Singh, 1980; Dibb et al., 1992, 1994; Liu et al., 2004, 2016) and subsidence (Feely
15 et al., 1989; Koch et al., 1996; Liu et al., 2004). Once produced, both radionuclides rapidly
16 ~~attach to ubiquitous submicron aerosol particles in the ambient air~~ (Papastefanou and
17 Ioannidou, 1995; Winkler et al., 1998; Gaffney et al., 2004; Ioannidou et al., 2005), and are
18 removed from the atmosphere mainly by wet and secondarily dry deposition (Kulan et al.,
19 2006). The concentrations of these radionuclides in surface air thus depend on their sources,
20 transport, wet and dry removal, and radioactive decay (in the case of ^7Be). Rainfall scavenging
21 processes are generally more effective on ^{210}Pb than on ^7Be concentrations (Koch et al., 1996;
22 Caillet et al., 2001; Likuku, 2006; Dueñas et al., 2009; Lozano et al., 2012).

23 Observational studies have previously been conducted to examine the factors influencing
24 surface ^{210}Pb and ^7Be concentrations in Europe, the Middle East and North Africa. Different

Deleted: attach onto aerosol particles in the fine fraction

1 synoptic and mesoscale patterns are associated with the ranges of ^{210}Pb and ^7Be activity
2 concentrations (Lozano et al., 2012, 2013). In southwestern Spain (El Arenosillo), for instance,
3 low ^{210}Pb values are strongly linked to air masses from the Atlantic Ocean, whereas the highest
4 values are associated with air masses clearly under the influence of continents, such as the
5 Iberian Peninsula and North of Africa (Lozano et al., 2012). As for ^7Be , the highest ^7Be activity
6 concentrations over southwestern Iberian Peninsula are related with the arrival of air masses
7 from middle latitudes, and in particular from the Canary Islands, western Mediterranean Basin
8 and the north of Africa (Dueñas et al., 2011; Lozano et al., 2012).

9 With respect to ^{210}Pb and ^7Be spatial variability, ^{210}Pb concentrations in surface air are
10 strongly dependent on whether it is located over land or ocean, whereas ^7Be concentration is
11 mainly latitudinally dependent, due to their different production mechanisms. Generally
12 speaking, in the Northern Hemisphere higher ^7Be concentrations are present at middle latitudes
13 (20-50° N), because of the mixing of stratospheric air into the upper troposphere along the
14 tropopause discontinuity in mid-latitude regions and subsequent convective mixing within the
15 troposphere, which brings ^7Be -rich air masses into the planetary boundary layer and to the
16 earth's surface (Kulan et al., 2006). Lower ^7Be concentrations are towards the pole and towards
17 the equator (Kulan et al., 2006; Steinmann et al., 2013).

18 Many studies examined the seasonal behavior of ^{210}Pb and ^7Be at European mid-latitude
19 surface sites (e.g., Cannizzaro et al., 1999; Ioannidou et al., 2005; Daish et al., 2005; Todorovic
20 et al., 2005; Likuku, 2006; Dueñas et al., 2009; Pham et al., 2011; Carvalho et al., 2013;
21 Steinmann et al., 2013). High levels of ^{210}Pb during summer and low levels in winter were
22 found, reflecting the differing rates of ^{222}Rn emanation from soil above the European land mass
23 during winter (wet or snow covered soil) and summer (dry soil) (Hötzl and Winkler, 1987;
24 Caillet et al., 2001; Daish et al., 2005; Ioannidou et al., 2005). At low-elevation sites, monthly

1 ^7Be averages are characterized by a well-defined annual cycle with lower values during winter
2 and higher values during summer. Generally, the increase of ^7Be in ground level air from March
3 to May is ascribed to the more efficient and higher frequency stratosphere- troposphere
4 exchange (STE), whereas the further increase of ^7Be during summer is due to the stronger
5 convective mixing and higher tropopause (Ioannidou et al., 2014). The higher tropopause
6 height is associated with anticyclonic conditions, which results in downward transport from the
7 upper troposphere and reduced wet scavenging during these conditions (Gerasopoulos et al.,
8 2001, 2005; Ioannidou et al., 2014). In fact, compensating subsidence associated with
9 convective mixing enhances downward transport of ^7Be from the upper troposphere (rather
10 than direct input of stratospheric air) down to the lower troposphere and ground level (Zanis et
11 al., 1999; Gerasopoulos et al., 2001, 2005; Ioannidou et al., 2005; Likuku et al., 2006;
12 Steinmann et al., 2013).

13 High-elevation sites such as Jungfrauoch (Switzerland), Zugspitze (Germany), and Mt.
14 Cimone (Italy), typically lying above the planetary boundary layer (PBL), are characterized by
15 lower ^{210}Pb concentrations and higher ^7Be due to direct influences of air masses from the free
16 troposphere (Zanis et al., 2000). The observed seasonal ^{210}Pb pattern at the [high-altitude](#) sites
17 of Puy de Dome (1465 m asl, France) and Opme (660 m asl, France) is characterized by
18 maximum concentrations in spring and autumn and minimum concentrations in winter. This is
19 due to higher radon emissions during the dry season (summer) than during the wet season
20 (winter), and lower PBL height during winter (Bourcier et al., 2011). The latter results in
21 weaker upward transport of ^{222}Rn and ^{210}Pb at high-altitude sites. Similar to low-elevation sites,
22 higher ^7Be values are observed in summer due to convection-forced exchange with the upper
23 troposphere and to the higher tropopause height that leads to more efficient vertical transport
24 from the upper to lower troposphere (Reiter et al., 1983; Gerasopoulos et al., 2001; Bourcier et
25 al., 2011). At high-altitude sites a secondary maximum of ^7Be during cold months (December-

Deleted: high altitude

1 March) is generally observed and attributed to the increase in stratosphere-to-troposphere
2 events during this season (e.g., James et al., 2003; Stohl et al., 2003; Trickl et al., 2010). The
3 higher frequency of rapid subsidence in winter at Northern Hemisphere mid-latitudes can be
4 ascribed to the intensity of baroclinic systems, which is greatest in the wintertime. In fact, well-
5 developed tropopause folds and rapid deep intrusions are most likely to occur in the wake of
6 intense cyclogenesis, usually limited to the wintertime storm track regions (James et al., 2003).

7 Numerical models have been used to analyze ^{210}Pb and ^7Be observations at high-elevation
8 sites. 1-D model simulations of surface ^7Be showed higher concentrations at high-elevation
9 sites (Jasiulionis and Wershofen, 2005; Simon et al., 2009), but also suggested that the diffusion
10 of ^7Be was affected by the seasonal variation of meteorological conditions. Balkanski et al.
11 (1993) examined the transport of ^{210}Pb in a global 3-D model and reported a weak decrease of
12 ^{210}Pb concentrations between the continental mixed layer and the free troposphere: simulated
13 concentrations at 6-km altitude were about 50% of those in the continental mixed-layer over
14 much of the Northern Hemisphere in summer, and over large areas of the tropics year around,
15 a result consistent with the few observations available for the free troposphere at that time
16 (Moore et al., 1973). Rehfeld and Heimann (1995) compared the 3-D model simulated seasonal
17 pattern of surface ^{210}Pb and ^7Be concentrations with the observations at several sites in both
18 hemispheres. At Mauna Loa (19.47°N, 155.6°W, 3400 m asl, Hawaii) ^{210}Pb seasonality was
19 characterized by high concentrations in spring and summer and lower ones in winter, as
20 opposed to the seasonal pattern found at higher latitudes, where the ^{210}Pb maximum
21 concentrations in winter are attributed to the advective transport of ^{210}Pb aerosols from mid-
22 latitudes. This behavior is due to the elevation of the site, representative of the conditions of
23 the free troposphere rather than those of the PBL. As for ^7Be , the comparison between the
24 model and the observations at Rexburg (43.8°N, 111.83°W, 1483 m asl, USA) showed
25 systematically lower model values, due to the much higher precipitation rates in the model.

1 Previous studies have examined surface ^7Be observations at Mt. Cimone with respect to
2 the role of STE in surface ozone increases (Bonasoni et al., 1999, 2000ab; Cristofanelli et al.,
3 2003, 2006, 2009a, 2015; Lee et al., 2007) within the framework of European projects such as
4 VOTALP (Vertical Ozone Transport in the Alps) and STACCATO (influence of Stratosphere-
5 Troposphere exchange in A Changing Climate on Atmospheric Transport and Oxidation
6 capacity). These studies led to the assessment of a higher incidence of STE events during the
7 period from October to February relative to the warm season, when thermal convection and the
8 rising of the tropopause promote vertical mixing, which acts as a confounding factor in STE
9 detection. Lee et al. (2007) and Tositti et al. (2014) reported the seasonal patterns and frequency
10 distributions of ^{210}Pb and ^7Be measured at Mt. Cimone, and highlighted higher concentrations
11 of both radionuclides in the summertime due to the higher mixing height and horizontal
12 transport by regional airflows. During winter, a general increase in ^7Be is associated with a
13 decrease in ^{210}Pb , due to the dominating effect of STE and subsidence in the free troposphere.
14 At the time of this work, no model analyses of ^{210}Pb and ^7Be observations at the site have been
15 conducted.

16 In this paper, we conduct simulations of ^{210}Pb and ^7Be at Mt. Cimone with a state-of- the-
17 art global 3-D chemistry and transport model (GMI CTM) driven by assimilated
18 meteorological fields for the year of 2005. Our objectives are a better elucidation of the
19 seasonal variations of ^{210}Pb and ^7Be concentrations and an improved understanding of the roles
20 of transport and precipitation scavenging processes in their seasonalities at Mt. Cimone.

21 The remainder of this paper is organized as follows. Section 2 describes the measurement
22 site, the radioactivity measurements at Mt. Cimone, and the GMI CTM. Section 3 evaluates
23 the model performance in reproducing the observed wind and precipitation fields. Section 4
24 evaluates the seasonal ^{210}Pb and ^7Be concentrations in the model with those observed. Section

1 5 examines the sources and seasonal variations in the simulated radionuclide activities,
2 followed by summary and conclusions in section 6.

3 **2 Data and Methods**

4 **2.1 Radionuclide Measurements at Mt. Cimone**

5 Mt. Cimone station (44°12' N, 10°42' E, 2165 m asl) is a global WMO-GAW station
6 managed by the Meteorological Office of the Italian Air Force, which hosts the research
7 platform “Ottavio Vittori” of the Institute of Atmospheric and Climate Science of the National
8 Council of Research (ISAC-CNR). The station is located on top of the highest peak of the
9 Italian northern Apennines, with a 360° free horizon and an elevation such that the station lies
10 above the PBL during most of the year: the Mt. Cimone measurements are considered
11 representative of the southern Europe/Mediterranean free troposphere (Bonasoni et al., 2000a;
12 Fischer et al., 2003; Cristofanelli et al., 2007), although during the warmer months an influence
13 of PBL air can be detected due both to convective processes and mountain/valley breeze
14 regimes (Fischer et al., 2003; van Dingenen et al., 2005; Tositti et al., 2013). Note in this
15 framework that southern Europe and Mediterranean basin are considered as a hot-spot region
16 in terms of both climate change (e.g., Forster et al., 2007) and air quality (Monks et al., 2009),
17 as well as a major crossroad of different air mass transport processes (Li et al., 2001; Lelieveld
18 et al., 2002; Millàn et al., 2006; Duncan et al., 2008; Tositti et al., 2013).

19 At Mt. Cimone station, ^{210}Pb , ^7Be , and aerosol mass load in the form of PM_{10} have been
20 regularly measured in the period of 1998-2011 with a Thermo-Environmental PM_{10} high-
21 volume sampler. PM_{10} is sampled on rectangular glass fiber filters (Whatman, 20.3 cm \times 25.4
22 cm, with an effective exposure area of about 407 cm²), which were manually changed every 2-
23 3 days, depending on weather conditions, failures of the sampling equipment and/or of the
24 power supply and personnel on site. The average flow rate was about 1.13 m³ min⁻¹ at standard

1 temperature and pressure (STP), with an average volume of air collected on each filter equal
2 to 3000-4000 m³ (about 48 hours of sampling, 115-175 samples per year).

3 Airborne radionuclides travel attached to particulate matters, and as a consequence of
4 their physical origin, tend to populate the fine fraction (<1.0 μm) (Winkler et al., 1998; Gaffney
5 et al., 2004). The PM₁₀ samples were subjected to non-destructive high-resolution γ-
6 spectrometry for the determination of airborne radiotracers ²¹⁰Pb and ⁷Be. The characteristics
7 of the two Hyper Pure Germanium crystal detectors (HPGe) detectors are as follows: one p-
8 type coaxial detector by Ortec/Ametek with a relative efficiency of 32.5% and FWHM 1.8 keV
9 at 1332 keV and one planar DSG detector with an active surface of 1500 mm² and FWHM 0.73
10 keV at 122 keV, for higher and lower energy ranges (100-2000 keV and 0-900 keV),
11 respectively.

12 Spectra were accumulated for at least one day to optimize peak analysis and then
13 processed with a specific software package (GammaVision-32, version 6.07, Ortec). Efficiency
14 calibration was determined on both detectors with a blank glass fiber filter traced with
15 accurately weighted aliquots of a standard solution of mixed radionuclides (QCY48,
16 Amersham) supplemented with ²¹⁰Pb, homogeneously dispersed dropwise over the filter
17 surface. Once dried under a hood under ambient conditions, the calibration filter was folded
18 into a polystyrene container in the same geometry as the unknown samples. Quantitative
19 analysis on samples was carried out by subtracting the spectrum of a blank filter in the same
20 geometry, while uncertainty on peaks (k = 1, 68% level of confidence) was calculated
21 propagating the combined error over the efficiency fit previously determined with the counting
22 error. Minimum detectable activity was calculated making use of the traditional ORTEC
23 method (ORTEC, 2003) with a peak cut-off limit of 40%. Activity data was corrected to the
24 midpoint of the time interval of collection and for the decay during spectrum acquisition. For
25 our analysis, we used monthly averages of ²¹⁰Pb and ⁷Be data at Mt. Cimone in 2005.

1 2.2 GMI Model

2 The Global Modeling Initiative (GMI, <http://gmi.gsfc.nasa.gov>) is a NASA-funded
3 project aiming at improving assessments of anthropogenic perturbations to the Earth system;
4 in this [framework](#), a CTM appropriate for stratospheric assessments was developed (Rotman
5 et al., 2001). It was firstly used to evaluate the potential effects of stratospheric aircraft on the
6 global stratosphere (Kinnison et al., 2001) and on the Antarctic lower stratosphere (Considine
7 et al., 2000). The recent version of the GMI CTM includes a full treatment of both stratospheric
8 and tropospheric photochemical and physical processes and is also capable of simulating
9 atmospheric radionuclides ^{222}Rn , ^{210}Pb , ^7Be , and ^{10}Be throughout the troposphere and
10 stratosphere (Considine et al., 2004, 2005; Rodriguez et al., 2004; Liu et al., 2016). Details of
11 the model are described in Duncan et al. (2007, 2008), Strahan et al. (2007), and Considine et
12 al. (2008).

Deleted: framework

13 In this work, ~~we simulate ^{222}Rn , ^{210}Pb , ^7Be , and ^{10}Be using~~ a version of the GMI model
14 with the same basic structure as described by Considine et al. (2005) and Liu et al. (2016),
15 including parameterizations of the important tropospheric physical processes such as
16 convection, wet scavenging, dry deposition and planetary boundary layer mixing.
17 Meteorological data used to drive the CTM ~~at 2° latitude by 2.5° longitude resolution~~, e.g.,
18 horizontal winds, convective mass fluxes and precipitation fields, are the Modern-Era
19 Retrospective analysis for Research and Applications (MERRA) assimilated data set from the
20 NASA Global Modeling and Assimilation Office (GMAO) (Rienecker et al., 2011).

Deleted: was used

21 The flux-form semi-Lagrangian advection scheme and a convective transport algorithm
22 from the CONVTRAN routine in NCAR CCM3 physics package are used in the model. The
23 wet deposition scheme is that of Liu et al. (2001): it includes scavenging in wet convective
24 updrafts, and first-order rainout and washout from both convective anvils and large-scale
25 precipitations. The gravitational settling effect of cloud ice particles included in Liu et al.

1 (2001) is not considered here. Dry deposition of aerosols is computed using the resistance-in-
2 series approach. For the simulations of radionuclides, each simulation was run for six years,
3 recycling the MERRA meteorological data for 2005, to equilibrate the lower stratosphere as
4 well as the troposphere (Liu et al., 2001). The sixth-year output was used for analysis.

Deleted: each year of the simulation

Deleted: sixth year

5 A uniform ^{222}Rn emission of $1.0 \text{ atom cm}^{-2} \text{ s}^{-1}$ from land under nonfreezing conditions is
6 assumed (Liu et al., 2001). Following Jacob and Prather (1990), the flux is reduced by a factor
7 of 3 under freezing conditions. The flux from oceans and ice is null. Although a large variability
8 of ^{222}Rn emission from land is observed, the above emission estimate is thought to be accurate
9 to within 25% globally (Turekian et al., 1977) and to within a factor of 2 regionally (Wilkening
10 et al., 1975; Schery et al., 1989; Graustein and Turekian, 1990; Nazaroff, 1992; Liu et al.,
11 2001).

12 Following Brost et al. (1991) and Koch et al. (1996), we used the Lal and Peters (1967)
13 ^7Be source for 1958 (solar maximum year), as it best simulated stratospheric ^7Be concentrations
14 measured from aircraft (Liu et al., 2001). The rates of ^7Be production reported more recently
15 by Usoskin and Kovaltsov (2008) broadly agree with those of Lal and Peters (1967) with
16 slightly (about 25%) lower global production rate and will be tested in a separate model study.
17 The Lal and Peters (1967) source is represented as a function of latitude and altitude (pressure)
18 and does not vary with season (see Figure 1 of Koch et al., 1996). No interannual variability in
19 the ^7Be source is considered in the model (Liu et al., 2001). This may lead to an underestimate
20 of tropospheric ^7Be concentrations, especially at high latitudes during a solar minimum (or near
21 minimum) year. Lal and Peters (1967) reported that the relative amplitude of the ^7Be production
22 rate over a 11-year solar cycle is about 13% below 300 hPa at latitudes above 45 degree.

23 Because of the coarse horizontal resolution of the model (2° latitude by 2.5° longitude),
24 the model representation of the topography at the site is poor. The elevation of Mt. Cimone in
25 the model is only 298 m, whereas in reality the mountain is 2165 m (asl) high (Figure 1). For

1 this reason, the model output was not sampled at ground level, but at the gridbox corresponding
2 to the elevation of the site. In order to see the sensitivity of model-observation comparisons to
3 spatial sampling, the model was sampled not only for the grid corresponding to the latitude and
4 longitude of Mt. Cimone, but also for the 8 adjacent grids. To better understand the sources
5 and seasonality of radiotracers in the model, we examine model output not only for ^{210}Pb , ^7Be
6 and their ratio $^7\text{Be}/^{210}\text{Pb}$ (an indicator of vertical transport [Koch et al., 1996]), which can be
7 directly compared to the measurements taken at Mt. Cimone, but also for other radiotracers and
8 quantities, e.g., ^{222}Rn , and $^{10}\text{Be}/^7\text{Be}$ (a STE tracer [Zanis et al., 2003]).

9 Year 2005 was chosen for analysis because of the availability of the observational data
10 and model output at the time of this work. As discussed later, the seasonal behavior of ^{210}Pb
11 and ^7Be radionuclides during year 2005 was “typical” for Mt. Cimone. Monthly averages of
12 ^{210}Pb and ^7Be data at Mt. Cimone were calculated for comparison with model results. To better
13 compare the seasonalities of ^{210}Pb and ^7Be between the model and the observations, the
14 monthly percentage deviations from the annual mean concentration were also calculated.

15 **3 Seasonal Variations of Transport and Precipitation at Mt. Cimone: Observations vs.** 16 **Model Simulations**

17 Mt. Cimone is the windiest meteorological station in Italy and the prevailing local winds
18 blow from S-SW and N-NE directions (Ciattaglia, 1983; Ciattaglia et al., 1987; Colombo et al.,
19 2000). The wind observations at Mt. Cimone during the period of 1998-2011, when
20 radionuclide measurements were performed at the station (Tositti et al., 2014), agree with the
21 climatology of local wind intensity and direction during the period of 1946-1999 as reported
22 by the Italian Air Force (Colombo et al., 2000). N-NE directions are more significant during
23 the cold period, and fluxes from SW are more typical of the warm period. While winds blowing
24 from the S-SW sector generate a sea air inflow, a continental air inflow is observed when winds
25 come from the N-NE sector (Ciattaglia et al., 1987).

1 However, when considering the lifetimes of ^{210}Pb (about one week) and ^7Be (about three
2 weeks) aerosols (Liu et al., 2001), it is apparent that the regional and long-range transport has
3 a much more important role than local transport. On a large scale, about 70% of background
4 air masses reaching Mt. Cimone in the period of 1996-1998 came from Atlantic and Arctic
5 areas, with a smaller contribution from the Mediterranean Basin and the eastern area, as
6 estimated by Bonasoni et al. (2000). A more recent and extended study of advection patterns
7 at Mt. Cimone (Brattich E. et al., “Advection patterns at the WMO-GAW station of Mt.
8 Cimone: seasonality, trends, and influence on atmospheric composition”, manuscript in
9 preparation, 2016), analyzing clusters of 4-day kinematic back-trajectories calculated for the
10 period of 1998-2011 with the HYSPLIT (HYbrid Single-Particle Lagrangian Integrated
11 Trajectory) model driven by the NCEP/NCAR (National Center for Environmental
12 Prediction/National Center for Atmospheric Research) meteorological reanalysis, shows that
13 the air masses advected to Mt. Cimone (55%) arrive from the Western-Atlantic-North America
14 sector, while the remaining air masses (from the Arctic, Eastern and Mediterranean Basin-
15 Northern Africa) together represent 45% of trajectories. Seasonal transport to Mt. Cimone in
16 the model is shown in Figure 2, representing winds at the elevation of Mt. Cimone (winds are
17 weaker at the model bottom layer). In agreement with the description of advection patterns at
18 the site, prevailing model winds (Figure 2) blow from the western-Atlantic sector. Slow
19 summer winds suggest the stronger influence of regional/local transport at Mt. Cimone during
20 the period (e.g., Lee et al., 2007; Marinoni et al., 2008; Tositti et al., 2013, 2014; Brattich et
21 al., 2015).

22 In the [model](#), Mt. Cimone appears to be in a location where there is a large horizontal
23 gradient of wind (transport) [during 2005](#). Long-range transport from Western Europe, North
24 America and Arctic region prevail during the cold period, while regional transport appears
25 more important in summer. The model is able to capture relevant features of pressure systems

Deleted: model

1 and seasonal circulation patterns of the North Atlantic/Mediterranean/African region, such as
2 the semi-permanent high pressure system located in the North Atlantic with different positions
3 during different seasons (Bermuda/Azores high), a semi-permanent system of high pressure
4 centered in northeastern Siberia during the colder half of the year (Siberian high), and the ITCZ
5 in the summer/autumn season. However, due to the coarse resolution of the global
6 meteorological reanalysis that we use to construct the model winds, the more than 50 local-
7 scale wind systems present in the Mediterranean and surrounding regions are not resolved
8 (Burlando, 2009). In northern Europe, in fact, there are approximately two main states for the
9 atmosphere, the westerly or zonal flows modulated by the advection of Atlantic lows, and the
10 long-lived blocking anticyclonic configurations over North Sea or Scandinavia (easterly)
11 (Burlando et al., 2008).

12 In the Mediterranean region, the main cyclones during winter are essentially sub-synoptic
13 lows triggered by the major North-Atlantic synoptic systems affected by the local topography
14 of the Northern Mediterranean coast (Trigo et al., 2002), whereas in summer cyclones develop
15 because of thermal effects, orography (e.g., the Atlas Mountains), and increase in low-level
16 thermal gradients (Trigo et al., 2002; Campins et al., 2006). Again, due to the coarse resolution
17 of the meteorological data we use, these sub-synoptic processes are not resolved. For instance,
18 North-African lows and Sahara depressions (also referred to as Atlas lee depressions) and the
19 resulting S-SW wind (Sirocco) (Reiter, 1975), potentially linked to ²¹⁰Pb variations at Mt.
20 Cimone, appear to be an important feature missing in the degraded MERRA data, where they

21 appear only during October/November. However, MERRA is able to capture the summertime
22 north-north easterly winds in the eastern Mediterranean (Aegean Sea), known as the Etesian
23 winds, generated by thermal effects.

24 We evaluate the MERRA precipitation with those from the GPCP (Global Precipitation
25 Climatology Project, <http://www.gewex.org/gpcp.html>) satellite and surface observations in

Formatted: Font: (Default) Times New Roman, 12 pt

Formatted: Font: (Default) Times New Roman, 12 pt

Formatted: Font: (Default) Times New Roman, 12 pt

Deleted: because of

Formatted: Font: (Default) Times New Roman, 12 pt

Formatted: Font: (Default) Times New Roman, 12 pt

1 2005. Figure 3 shows the MERRA and GPCP monthly precipitation for the region defined by
2 0-75°N and 90°W – 90°E. A good agreement between the MERRA and the GPCP
3 precipitations averaged over the region was found. In particular, summer precipitation patterns
4 are very similar. The geographical distribution of precipitation in MERRA shows some
5 important features in agreement with the observed climatology precipitations: the desert
6 climate in North Africa with very low precipitation all year long, the ITCZ with high
7 precipitation during the summer/autumn seasons, the North Atlantic region with high
8 precipitation especially during the winter and autumn seasons, and Europe where the seasonal
9 pattern of precipitation is similar to that in the North Atlantic region, but precipitation is lower.

10 Figure 4 shows the comparison of the GPCP and MERRA precipitation seasonality at Mt.
11 Cimone. Since Mt. Cimone is located in a region with a large horizontal gradient in
12 precipitation, we also show in the figure the comparisons for three adjacent gridboxes. The
13 MERRA precipitation is generally lower than that of GPCP at two gridboxes (except for
14 summer, Figure 4ab), but in good agreement at the other two gridboxes (Figure 4cd). The
15 agreement between the MERRA and GPCP precipitation seasonality is reasonable, with the
16 squared correlation coefficient R^2 varying between 0.56 (at the grid to the northwest of “ij”) and
17 0.89 (at the grid to the southeast of “ij”). Large differences between the MERRA
18 precipitation and that locally observed at the station are instead present. While the daily mean
19 observed 2005 precipitation is 0.81 mm, which is close to the corresponding precipitation (0.73
20 mm) in MERRA at the “ij” grid (i.e., a negative bias of -0.08 mm); the model bias is positive
21 and much higher (0.31 – 1.28 mm) at adjacent grids. This bias may very well reflect again the
22 fact that the observed surface precipitation is localized, whereas the satellite and MERRA
23 precipitations correspond to a much larger scale (about 200 km). Moreover, as Colombo et al.
24 (2000) previously pointed out, different from the surrounding area where the climate is defined
25 as temperate-continental, the climate at the mountaintop is classified as alpine because of the

Deleted: (not shown): in particular, the MERRA precipitation is larger during winter-autumn, while it is much more similar to that observed during spring-summer.

Deleted:

Deleted: difference

1 high elevation. In fact, in agreement with the GPCP precipitation in 2005, the observed
2 climatology in the region shows maximum during November (secondary maximum in spring)
3 and absolute minimum in July (secondary minimum in January), whereas on the top of the
4 mountain the precipitation is maximal during summer. The MERRA precipitation shows
5 increased amounts during April and August-December, with minimum in June-July. As the
6 local precipitation at the site is important to the scavenging of radionuclide aerosol tracers, this
7 difference between the local and regional precipitation could contribute to any biases in our
8 simulations. However, as we will show below, the ratio $^7\text{Be}/^{210}\text{Pb}$ may cancel out the errors
9 associated to precipitation scavenging (Koch et al., 1996).

10 Low ^{210}Pb concentrations are seen over the Atlantic Ocean, due to the negligible
11 emissions of ^{222}Rn from the oceans and strong precipitation scavenging, and in northern and
12 western Europe especially during the cold season (Figure 2a). High ^{210}Pb concentrations appear
13 over the [Sahara Desert](#) and North Africa, as a result of low precipitation in this area, and also
14 over the Middle East and South Asia. ^{210}Pb concentrations over southern Europe appear higher
15 during the transition seasons, especially fall, and peak during summer when the minimum
16 precipitation and slow winds from west are observed in the region. Low ^7Be concentrations are
17 simulated along the equator where convective scavenging is strongest (Figure 2b). High ^7Be
18 concentrations are seen over the [Sahara Desert](#) due to a combination of low precipitation and
19 subsidence in this region. Elevated values also occur over the Middle East, North America, and
20 Greenland. ^7Be concentrations over southern Europe appear higher during spring and peak
21 during winter, when model winds are stronger and transport ^7Be aerosols from North America
22 and Greenland regions where ^7Be production is highest (Beer et al., 2012).

23 **4 Seasonal Variations of ^{210}Pb and ^7Be at Mt. Cimone: Observations vs. Model** 24 **Simulations**

Deleted: Sahara desert

Deleted: Sahara desert

1 The seasonality and frequency distributions of ^{210}Pb and ^7Be concentrations measured at
2 the Mt. Cimone station were previously examined by Lee et al. (2007), while more recent
3 analyses of the 12-year record were presented in Tositti et al. (2014) and Brattich et al. (2015).
4 Generally, both radionuclides show a marked seasonal maximum in the summertime, a
5 behaviour shared by PM_{10} (Tositti et al., 2013) and O_3 (Bonasoni et al., 2000b). ^{210}Pb summer
6 maximum is mainly due to the higher mixing height and enhanced uplift from the boundary
7 layer as a result of thermal convection. The seasonal fluctuation of ^7Be is more complex and
8 characterized by two relative maxima, one during the cold season associated with stratosphere-
9 to-troposphere transport, and the other during the warm season mainly associated with
10 tropospheric subsidence balancing lower-tropospheric air masses ascent occasionally
11 accompanied by STE (Tositti et al., 2014). The ^{210}Pb and ^7Be measurements in 2005 are
12 consistent with this description (Figure 5): ^{210}Pb concentrations are characterized by two
13 maxima during the warm period (July and September); ^7Be concentrations are characterized by
14 one absolute maximum during summer (July) and one secondary maximum during spring
15 (March).

16 Figure 5 (ab) compares the simulated monthly ^{210}Pb and ^7Be activities with the
17 observations at Mt. Cimone in 2005. The comparisons for the monthly percentage deviations
18 from the annual mean concentration are available as Supplementary Information (hereafter SI,
19 SI Figures 1-2). The seasonality of ^{210}Pb is well captured by the model. The model reproduces
20 the presence of two seasonal maxima in the ^{210}Pb observations, with the maximum observed in
21 July shifted to June in the simulation. The squared correlation coefficient R^2 between observed
22 and simulated ^{210}Pb activities is equal to 0.83 at the “ij” grid and varies between 0.42 and 0.82
23 for adjacent gridboxes (to the north and to the west of “ij”, respectively), confirming the good
24 performance of the model in reproducing the ^{210}Pb seasonal pattern.

1 As for ^7Be , the model well captures the March maximum (i.e., secondary maximum in
2 the observations) and the month-to-month variation during the cold and transition seasons
3 (January-April, October-December). However, during the warm period, the simulated ^7Be
4 concentrations are lower by a factor of 2 than the observed. A better agreement was found at
5 some adjacent model gridboxes (e.g., to the south and to the southwest of “ij”; Figure 6 vs.
6 Figure 5). The correlation between observed and simulated monthly ^7Be activities also
7 increases from $R^2 = 0.03$ at “ij” to $R^2 = 0.11-0.60$ at adjacent model gridboxes. The largest
8 value of $R^2 = 0.6$ was obtained at the “ij-1” gridbox to the south of “ij” (Figure 6). This
9 improvement is due to the large horizontal gradient in the simulated ^7Be concentrations near
10 the site (Figure 2).

Deleted: general seasonal pattern

Deleted: “

12 5 Sources and Seasonality of ^{210}Pb and ^7Be at Mt. Cimone: A Model Analysis

13 In this section, we quantify the sources of ^{210}Pb and ^7Be and determine the processes
14 governing their seasonality in the GMI model. Additional tracers as simulated by the model are
15 used to aid in the interpretation. Model sensitivity experiments are conducted to examine the
16 roles of transport and precipitation scavenging in the seasonality.

17 As discussed in Section 4, the model well reproduces the ^{210}Pb seasonality, with
18 minimum in the cold period and maximum in the warm period. The ^{210}Pb seasonality (Figure
19 5a) can be linked with the seasonal pattern of its precursor ^{222}Rn (Figure 5c). It is seen that the
20 summer ^{210}Pb maximum is due to stronger (thermal) convection, which uplifts more ^{222}Rn out
21 of the boundary layer (e.g., Lee et al., 2007; Tositti et al., 2014; Brattich et al., 2015). This
22 uplift of ^{222}Rn from the boundary layer is minimum in the cold period, and the minimal level
23 of ^{210}Pb in this period can be considered representative of the free troposphere. The ^{210}Pb
24 summer increase appears to be associated with short-range and regional transport, as suggested
25 by the model simulations (Figure 2a). As expected, long-range transport is more typical of the

1 winter/spring seasons because of stronger horizontal winds, while regional effects are more
2 important during summer when convection gets stronger.

3 In a similar manner, the source of the ^7Be March maximum can be investigated with
4 model tracer simulations. Figure 5 (de) also shows the simulated seasonal patterns of the
5 $^{10}\text{Be}/^7\text{Be}$ activity ratio and of the fraction of ^7Be originating from the stratosphere (strat
6 $^7\text{Be}/\text{total } ^7\text{Be}$). The simulated seasonal pattern of the $^{10}\text{Be}/^7\text{Be}$ ratio is very similar to the
7 observations at Jungfraujoch (Switzerland, 3580 m asl) (Zanis et al., 2003), characterized by a
8 clear seasonal cycle with peak ratios in spring. The usefulness of $^{10}\text{Be}/^7\text{Be}$ ratio as a
9 stratospheric tracer is due to the fact that both ^{10}Be and ^7Be cosmogenic radionuclides attach
10 to the same aerosols and share therefore the same removal mechanism. Moreover, due to the
11 much longer physical half-life of ^{10}Be ($\tau_{1/2} = 1.5 \times 10^6$ years) compared to ^7Be ($\tau_{1/2} = 53.3$
12 days), their concentration ratios in the stratosphere (about 3-4) are much higher than in the
13 troposphere (about 2 or even less) (Koch and Rind, 1998). The simulated $^{10}\text{Be}/^7\text{Be}$ ratio
14 behavior indicates that deep stratosphere-to-troposphere (STT) peaks during winter, while
15 shallower STT has a spring maximum, consistent with previous analyses of stratospheric
16 intrusions at Mt. Cimone (Cristofanelli et al., 2006, 2009), and more generally with the
17 climatology of stratosphere-troposphere exchange at the Northern Hemisphere mid-latitudes
18 (James et al., 2003). Altogether the simulated high strat $^7\text{Be}/\text{total } ^7\text{Be}$, high $^7\text{Be}/^{210}\text{Pb}$ (Figure
19 7), and low $^{10}\text{Be}/^7\text{Be}$ ratios during December-January indicate strongest STE during this period,
20 followed by spring with slightly weaker stratospheric influence on surface ^7Be . However, the
21 model tends to overestimate the observed ^7Be concentrations and $^7\text{Be}/^{210}\text{Pb}$ ratios during
22 December-February, suggesting that stratospheric influence and/or subsidence in the model is
23 probably too strong in this region at this time of the year. It is noted that globally integrated
24 STT mass fluxes in the MERRA reanalysis are actually smaller than in some other reanalyses,
25 e.g., ERA-Interim, JRA-55, and MERRA-2 (Boothe and Homeyer, 2016).

Deleted: Zugspitze

Deleted: Germany

Deleted: 2962

Deleted: not-pronounced

Deleted: somewhat elevated

Deleted: February-April and June-July

Formatted: Font color: Red

Deleted: Heini

Formatted: Font color: Red

Deleted: STE

Formatted: Font color: Red

Deleted: likely

Formatted: Font color: Red

Deleted: fast

Formatted: Font color: Red

1 The use of the ^7Be production rate of Lal and Peters (1967) for a solar maximum year
2 (1958) may partly explain the lower annual mean ^7Be in the model (3.4 mBq m^{-3} annual mean
3 at the “ij” grid) than in the observations (4.2 mBq m^{-3}). In fact, the sunspot number in 2005
4 (29.8) was quite low (slowly decreasing from 2000, a solar maximum year, and reaching
5 minimum in 2008), especially compared to the 1958 value of 184.8. Sunspot number data are
6 available from the World Data Center for the production, preservation and dissemination of the
7 international sunspot number (Sunspot Index and Long-term Solar Observation, SILSO, Royal
8 Observatory of Belgium, Brussels, <http://sidc.oma.be/sunspot-data/>).

9 During the winter period, associated with the simulated and observed ^7Be increases
10 (Figures 5-6), strong long-range transport was dominant in the European region (Figure 2b).
11 Transport from higher latitude regions (Arctic, northern Europe, and North America) appears
12 particularly important during this period (Figure 2b); such transport from high-latitude regions,
13 where the ^7Be production rate is highest (Beer et al., 2012), has typically been observed during
14 STE events at Mt. Cimone in many studies (e.g., Bonasoni et al., 1999, 2000ab).

15 The discrepancy between the simulated and the observed ^7Be concentrations during the
16 warm period is partly due to the sensitivity to spatial sampling in the model. As seen from the
17 map plots of ^{210}Pb and ^7Be concentrations at the elevation of Mt. Cimone (Figure 2), the
18 sampling site appears to be located in a region where the N-S gradient of concentrations is large
19 (especially for ^7Be). An elevated gradient in the region surrounding Mt. Cimone was also seen
20 for winds, as transport plays a critical role in determining the distributions of these tracers. The
21 sensitivity to spatial sampling in the model is therefore ascribed to this observed strong gradient
22 in the N-S direction. In fact, while the grids to the south and southwest of “ij” are better for
23 summer ^7Be comparisons (Figure 6), the grids to the northeast, north, and northwest of “ij” are
24 better for winter (not shown).

Deleted: . As reported by Huang et al. (2013), a stronger net subsidence of air masses to the surface could be due to unrealistic meteorological conditions (e.g., boundary layer structure, wind fields, vertical mixing).¶

Formatted: Font color: Red

1 The model underestimate of ^7Be levels in the warm months may also suggest the mixing
2 of air masses between the PBL and the lower free troposphere is likely too weak. Previous
3 observational analyses indicated that such mixing is higher in summer at Mt. Cimone due to
4 enhanced convection and mountain wind breeze (e.g., Fischer et al., 2003; Cristofanelli et al.,
5 2007). Weaker entrainment of free-tropospheric air into the PBL would result in lower ^7Be
6 concentrations at the surface.

7 The model annual average biases are about 8% for ^{210}Pb and about 19% for ^7Be ,
8 respectively. By contrast, the model average bias for $^7\text{Be}/^{210}\text{Pb}$ ratios is about -13% (Figure 7).
9 The smaller model bias for $^7\text{Be}/^{210}\text{Pb}$ ratios than for ^7Be concentrations reflects the fact that the
10 ratio cancels out the errors in precipitation scavenging (Koch et al. 1996) that contribute to the
11 underestimate of ^{210}Pb and ^7Be activities. On the other hand, the negative model bias for the
12 $^7\text{Be}/^{210}\text{Pb}$ ratio again points to weak downward mixing from the free troposphere.

13 If one compares the month-to-month variation of ^{210}Pb and ^7Be (Figures 5 and 6) and
14 precipitation in the model (Figure 4), the maxima/minima of precipitation appear to be in phase
15 with those of both radionuclides' activities. This reflects the effects of precipitation scavenging
16 on radionuclide aerosols.

17 We conducted model sensitivity experiments where convection (transport and
18 scavenging), wet scavenging due to both large-scale and convective precipitation, and dry
19 deposition processes are turned off, respectively, to examine the roles of these processes in
20 controlling the seasonality of ^{210}Pb and ^7Be at Mt. Cimone. Figure 8 shows the results for the
21 standard and sensitivity runs at the “grid to the south of “ij”, for which the simulated tracer
22 seasonal variations are similar to those observed, while the monthly percentage deviations from
23 the annual mean concentrations are shown in SI Figure 3. Figures 9-12 show maps of simulated
24 changes in ^{210}Pb and ^7Be concentrations when convection or wet scavenging is turned off.

1 Turning off dry deposition does not significantly change the simulated ^{210}Pb and ^7Be
2 concentrations, partly due to sampling the higher vertical gridbox in the model (larger effects
3 are seen at the bottom model layer). Turning off convection (i.e., with neither convective
4 transport nor convective scavenging), the simulated ^7Be seasonality also remains nearly the
5 same. This suggests the compensating effects between subsidence (increasing ^7Be) associated
6 with convective transport and scavenging (decreasing ^7Be) due to convective precipitation. In
7 the case of ^{210}Pb , turning off convection does not change the seasonal pattern but generally
8 results in larger ^{210}Pb concentrations and particularly during summer/autumn when convective
9 transport is more important at the site. In fact, no convective transport of ^{222}Rn (SI Figure 5)
10 results in less ^{222}Rn (and ^{210}Pb) being transported to the free troposphere, but also more ^{210}Pb
11 available in PBL lifted to the free troposphere by large-scale vertical transport; on the other
12 hand, lack of convective scavenging of ^{210}Pb increases its concentration in the free troposphere.
13 Turning off convection therefore results in an increase of ^{210}Pb concentrations in the free
14 troposphere. Both surface ^{222}Rn concentrations at the elevation of Mt. Cimone (SI Figure 4),
15 as well as a map of changes in ^{210}Pb concentrations due to convection in the model (Figure 9)
16 show that convection in the region is more important during summer and autumn, but is not
17 negligible during spring, possibly due to thermal inertia.

18 The model run without scavenging suggests that, apart from downward transport from
19 the upper troposphere and lower stratosphere, wet scavenging is mainly responsible for the
20 seasonal variation of ^7Be (Figure 8, bottom panel). None of our simulations is able to describe
21 the observed ^7Be summertime peak, suggesting that local and regional circulations in this
22 region with complex topography may not be resolved by the coarse-resolution model. For ^{210}Pb
23 (Figure 8, top panel), it appears that wet scavenging plays a more important role during August-
24 December than during January-July. This appears to be associated with the seasonality of
25 precipitation, which shows prolonged elevated values during August-December, as well as a

Deleted: the

1 maximum during April, as previously discussed (Figure 5). A plot of changes in ^{210}Pb
2 concentrations due to scavenging in the model (Figure 10) confirms that the scavenging effect
3 is larger during fall and, to a lesser extent, during summer. At Mt. Cimone, the scavenging
4 effect is not minimal during July (month of minimum precipitation, Figure 4), suggesting the
5 influence of precipitation scavenging elsewhere in the region on the site.

6 **6 Summary and Conclusions**

7 We have used a global 3-D model (GMI CTM) driven by the MERRA assimilated
8 meteorological data from NASA's GMAO to simulate the ^{210}Pb and ^7Be observations from the
9 Mt. Cimone (44°12' N, 10°42' E, 2165 m asl, Italy) WMO-GAW station in 2005. The two
10 natural atmospheric radionuclides originate from contrasting source regions (lower troposphere
11 and upper troposphere/lower stratosphere, respectively), attach to submicron particles, and are
12 removed from the troposphere mainly by wet deposition. Our objective was to examine the
13 roles of horizontal advection, vertical transport (large-scale and convection), and wet
14 scavenging in determining the seasonality of ^{210}Pb and ^7Be at Mt. Cimone. The observed ^{210}Pb
15 concentrations are characterized by maxima in summer and minima during the cold period.
16 The seasonality of ^7Be is more complex, with a major peak in summer, a secondary peak in
17 spring and a minimum in winter. This is the first modeling study of ^{210}Pb and ^7Be observations
18 at Mt. Cimone. This site is representative of free-tropospheric Southern Europe/Mediterranean
19 conditions most of the year, and as such the comparison between measurements and
20 simulations can serve as an indication of shortcomings in the model or in the meteorological
21 data.

22 Precipitation and wind fields are important to the model's performance in representing
23 the transport and scavenging processes. We evaluated the MERRA precipitation field used by
24 GMI CTM against the GPCP satellite and surface observations, and a generally good
25 agreement was found. The seasonality of precipitation at Mt. Cimone shows increased amounts

1 during April and the period of August-December, and minimum in June-July. The MERRA
2 assimilated winds at the [low-resolution](#) version we used captured the main circulation patterns
3 (e.g., location of the Azores high pressure, location of the ITCZ) in the Northern Hemisphere.
4 However, some local-scale winds and pressure systems, which are important for transport to
5 the sampling site, were likely not well resolved at the coarse resolution we used. A general
6 good agreement was found between the MERRA assimilated wind fields and the main
7 advection patterns at the site (e.g., prevalence of long-range transport from Western Europe,
8 North America and Arctic region during the cold season, as opposed to the prevailing regional
9 transport during the warm season).

Deleted: low resolution

10 The model well reproduced the observed ^{210}Pb seasonality: ^{210}Pb maxima during the
11 warm period were attributed to the stronger (thermal) convection, which uplifts more ^{222}Rn
12 (and ^{210}Pb) from the boundary layer. The model is less successful in reproducing the observed
13 ^7Be seasonality. ^7Be was better represented during the cold period, while the observed summer
14 ^7Be maximum was underestimated by the model. The model underestimate of ^7Be levels in the
15 warm months is partly due to the sensitivity to spatial sampling in the model, but also suggests
16 that the mixing of air masses between the PBL and the lower free troposphere ([e.g., via](#)
17 [convection and compensating subsidence](#)) is likely too weak [during summer when the Mt.](#)
18 [Cimone station is located within the PBL](#). This suggests that additional work comparing the
19 model results with more surface observations is needed in order to better understand this effect.
20 The simulated lower annual average ^7Be concentration relative to the observation is also partly
21 attributed to the fact that the model used the ^7Be production rate for a solar maximum year,
22 while in 2005 (our simulation year) the solar activity was rather low.

23 By examining the wind fields and horizontal distribution of radiotracers in the model, we
24 noted that the sampling site is in a location where there is a large gradient, especially in the
25 North-South direction. Accordingly, we investigated the sensitivity of model results to spatial

1 sampling. A better agreement between the model and the observations at some adjacent
2 gridboxes was found. The ^7Be March maximum was linked to the large stratospheric influence
3 during winter/spring. The model tends to underestimate the summertime ^{210}Pb and ^7Be , but
4 better simulates the $^7\text{Be}/^{210}\text{Pb}$ ratio because the model errors due to precipitation scavenging
5 appear to be canceled out in the ratio.

6 We have conducted a series of model sensitivity experiments to further examine and
7 quantify the roles of wet scavenging, dry deposition, and convection (transport and scavenging)
8 in controlling the seasonality of ^{210}Pb and ^7Be at Mt. Cimone. Dry deposition does not have a
9 significant effect on the magnitude and seasonality of ^{210}Pb and ^7Be concentrations at the site.
10 The relatively weak combined effects of convective transport and convective scavenging on
11 the radiotracer seasonality were attributed to the compensating effects of convective transport
12 and convective scavenging on tracer concentrations in the lower free troposphere (at the
13 elevation of Mt. Cimone). Convection appears to be more important to the regional distribution
14 of both radiotracers during summer and autumn, although it is also significant during spring.
15 Finally, scavenging is found to be the most important process controlling the seasonal
16 variations of ^{210}Pb and ^7Be at Mt. Cimone. For ^{210}Pb , precipitation plays a more important role
17 during August-December than during January-July. This was attributed to the seasonality of
18 local and regional precipitation, which shows prolonged elevated values in the period of
19 August-December.

20 While our simulations demonstrated some capabilities of the model to reproduce the
21 seasonality of ^{210}Pb and ^7Be , they highlight the weaknesses of the model in reproducing local
22 features, presumably due to its coarse resolution. Model simulations at a higher resolution
23 would improve this model analysis of ^{210}Pb and ^7Be observations at Mt. Cimone, a high-
24 elevation site. The understanding of downward transport associated with convection during
25 summer also requires improving. As such, ^{210}Pb and ^7Be tracers will prove to be very useful in

1 our understanding of seasonal behaviors of other environmentally important trace gases and
2 aerosols at Mt. Cimone. Since other aerosols and trace gases (e.g., black carbon, CO, O₃) are
3 also measured at the station, we plan to conduct comparisons between model simulations and
4 those measurements to corroborate or contrast with the radionuclide results.

5

6 **Data availability**

7 A description of the observational data and model output used in this paper can be found in
8 Sect. 2 and they are available upon request by contacting Laura Tositti (laura.tositti@unibo.it)
9 and Hongyu Liu (hongyu.liu-1@nasa.gov), respectively.

10

11 **Acknowledgements.** Italian Air Force Meteorological Office (IAFMS) and ISAC-CNR are
12 gratefully acknowledged for their precious technical support at the Mt. Cimone station. In
13 particular, ISAC-CNR is gratefully acknowledged for providing infrastructural access at the
14 WMO-GAW Global Station Italian Climate Observatory "O. Vittori" at Mt. Cimone. IAFMS
15 is gratefully acknowledged for providing meteorological observations at Mt. Cimone station.
16 The Italian Climate Observatory "O. Vittori" is supported by MIUR and DTA-CNR throughout
17 the Project of National Interest NextData. Erika Brattich thanks the National Institute of
18 Aerospace (NIA) Visitor Program for hosting her one month visit, and the Department of
19 Biological, Geological and Earth Sciences of the University of Bologna for grant support
20 during her PhD study. Hongyu Liu is supported by NASA Modeling and Analysis Program
21 (MAP), NASA Atmospheric Composition Modeling and Analysis Program (ACMAP), and
22 NASA Atmospheric Composition Campaign Data Analysis and Modeling (ACCDAM)
23 program. The GMI activity is managed by José Rodriguez and Susan Strahan (NASA GSFC).
24 Stephen Steenrod, Megan Damon, and Jules Kouatchou (GSFC) are acknowledged for

1 programming support. NASA Center for Computational Sciences (NCCS) provided
2 supercomputing resources.

3

4 **References**

5 Arimoto, R., Snow, J.A., Graustein, W.C., Moody, J.L., Ray, B.J., Duce, R.A., Turekian, K.K.,
6 and Maring H.B.: Influences of atmospheric transport pathways on radionuclide activities
7 in aerosol particles from over the North Atlantic, *J Geophys Res*, 104(D17), 301-321, 1999.

8 Balkanski, Y, Jacob, D.J., Gardner, G.M., Graustein, W., Turekian, K.K.: Transport and
9 residence times of tropospheric aerosols inferred from a global three-dimensional
10 simulation of ^{210}Pb , *J Geophys Res*, 98 (D11), 20573-20586, 1993.

11 Baskaran, M.: Po-210 and Pb-210 as atmospheric tracers and global atmospheric Pb-210
12 fallout: a review, *J Environ Radioactiv*, 102, 500-513, 2011.

13 Beer, J., McCracken, K., and von Steiger, R.: *Cosmogenic radionuclides*. Springer, Heidelberg,
14 Germany, 2012.

15 Bonasoni, P., Evangelisti, F., Bonafé, U., Feldmann, H., Memmesheimer, M., Stohl, A., and
16 Tositti, L.: Stratosphere-troposphere exchanges: case studies recorded at Mt. Cimone
17 during VOTALP project, *Phys Chem Earth (C)*, 24(5), 443-446, 1999.

18 Bonasoni, P., Evangelisti, F., Bonafé, U., Ravegnani, F., Calzolari, F., Stohl, A., Tositti, L.,
19 Tubertini, O., and Colombo, T.: Stratospheric ozone intrusion episodes recorded at Mt.
20 Cimone during VOTALP project: Case studies, *Atmos Environ*, 34, 1355-1365, 2000a.

21 Bonasoni, P., Stohl, A., Cristofanelli, P., Calzolari, F., Colombo, T., and Evangelisti, F.:
22 Background ozone variations at Mt Cimone station, *Atmos Environ*, 34, 5183-5189, 2000b.

23 [Boothe, A. C. and Homeyer, C. R.: Global large-scale stratosphere-troposphere exchange in](#)
24 [modern reanalyses, *Atmos. Chem. Phys. Discuss.*, doi:10.5194/acp-2016-788, in review,](#)
25 [2016.](#)

1 Bourcier, L., Masson, O., Laj, P., Pichon, J.M., Paulat, P., Freney, E., and Sellegri, K.:
2 Comparative trends and seasonal variation of ^7Be , ^{210}Pb and ^{137}Cs at two altitude sites in
3 the central part of France, *J Environ Radioactiv*, 102, 294-301, 2011.

4 Brattich, E., Hernández-Ceballos, M.A., Cinelli, G., and Tositti, L.: Analysis of peak ^{210}Pb
5 values at Mt. Cimone (1998-2011), *Atmos Environ*, 112, 136-147, 2015.

6 Brattich, E., Orza, J.A.G., and Tositti, L.: Advection patterns at the WMO-GAW station of Mt.
7 Cimone: seasonality, trends, and influence on atmospheric composition, manuscript in
8 preparation, 2016.

9 Brost, R.A., Feichter, J., and Heimann, H.: Three-dimensional simulation of ^7Be in a global
10 climate model, *J Geophys Res*, 96, 22423-22445, 1991.

11 Burlando, M.: The synoptic-scale surface wind climate regimes of the Mediterranean Sea
12 according to the cluster analysis of ERA-40 wind fields, *Theor Appl Climatol*, 96, 69-83,
13 2009.

14 Burlando, M., Antonelli, M., and Ratto, C.F.: Mesoscale wind climate analysis: identification
15 of anemological regions and wind regimes, *Int J Climatol*, 28, 629-641, 2008.

16 Caillet, S., Arpagaus, P., Monna, F., and Dominik, J.: Factors controlling ^7Be and ^{210}Pb
17 atmospheric deposition as revealed by sampling individual rain events in the region of
18 Geneva, Switzerland, *J Environ Radioactiv*, 53, 241-256, 2001.

19 Campins, J., Jansà, A., and Genovés, A.: Three-dimensional structure of western
20 Mediterranean cyclones, *Int J Climatol*, 26, 323-343, 2006.

21 Cannizzaro, F., Greco, G., Raneli, M., Spitale, M.C., and Tomarchio, E.: Concentration
22 measurements of ^7Be at ground level air at Palermo, Italy – comparison with solar activity
23 over a period of 21 years, *J Environ Radioactiv*, 84, 457-467, 2004.

1 Carvalho, A.C., Reis, M., Silva, L., and Madruga, M.J.: A decade of ^7Be and ^{210}Pb activity in
2 surface aerosols measured over the Western Iberian Peninsula, *Atmos Environ*, 67, 193-
3 202, 2013.

4 Ciattaglia, L.: Interpretation of atmospheric CO₂ measurements at Mt. Cimone (Italy) related
5 to wind data. *Journal of Geophysical Research* 88, C2, 1331-1338, 1983.

6 Ciattaglia, L., Cundari, V., and Colombo, T.: Further measurements of atmospheric carbon
7 dioxide at Mt. Cimone, Italy: 1979-1985, *Tellus B*, 39, 13-20, 1987.

8 Colombo, T., Santaguida, R., Capasso, A., Calzolari, F., Evangelisti, F., and Bonasoni, P.:
9 Biospheric influence on carbon dioxide measurements in Italy, *Atmos Environ*, 34, 4963-
10 4969, 2000.

11 Considine, D.B., Douglass, A.R., Connell, P.S., Kinnison, D.E., and Rotman, D.A.: A polar
12 stratospheric cloud parameterization for the global modeling initiative three-dimensional
13 model and its response to stratospheric aircraft, *J Geophys Res*, 105(D3), 3955-3973, 2000.

14 Considine, D.B., Connell, P.S., Logan, J.A.: Simulating ozone in the near tropopause region
15 with a new combined model of the stratosphere and troposphere, in: *Quadrennial Ozone*
16 *Symposium QOS 2004*, edited by: Zerefos, C, International Ozone Commission, Kos,
17 Greece, pp. 739-740, 2004.

18 Considine, D.B., Bergmann, D.J., and Liu, H.: Sensitivity of Global Modeling Initiative
19 chemistry and transport model simulations of radon-222 and lead-210 to input
20 meteorological data, *Atmos Chem Phys*, 5, 3389-3406, 2005.

21 Cristofanelli, P., Bonasoni, P., Collins, W., Feichter, J., Forster, C., James, P., Kentarchos, A.,
22 Kubik, P.W., Land, C., Meloan, J., Roelofs, G.J., Siegmund, P., Sprenger, M., Schnabel,
23 C., Stohl, A., Tobler, L., Tositti, L., Trickl, T., and Zanis, P.: Stratosphere-to-troposphere
24 transport: A model and method evaluation, *J Geophys Res*, 108(D12), 8525,
25 doi:10.1029/2002JD002600, 2003.

1 Cristofanelli, P., Bonasoni, P., Tositti, L., Bonafé, U., Calzolari, F., Evangelisti, F., Sandrini,
2 S., and Stohl, A.: A 6-year analysis of stratospheric intrusions and their influence on ozone
3 at Mt. Cimone (2165 m above sea level), *J Geophys Res*, 111, D03306,
4 doi:10.1029/2005JD006553, 2006.

5 Cristofanelli, P., Bonasoni, P., Carboni, G., Calzolari, F., Casarola, L., Zauli Sajani, S., and
6 Santaguida, R.: Anomalous high ozone concentrations recorded at a high mountain station
7 in Italy in summer 2003, *Atmos Environ*, 41, 1383-1394, 2007.

8 Cristofanelli, P., Calzolari, F., Bonafé, U., Duchi, R., Marinoni, A., Roccatò, F., Tositti, L., and
9 Bonasoni P.: Stratospheric intrusion index (SI^2) from baseline measurement data, *Theor*
10 *Appl Climatol*, 97, 317-325, 2009a.

11 Cristofanelli, P., Marinoni, A., Arduini, J., Bonafé, U., Calzolari, F., Colombo, T., Decesari,
12 S., Duchi, R., Facchini, M.C., Fierli, F., Finessi, E., Maione, M., Chiari, M., Calzolari, G.,
13 Messina, P., Orlandi, E., Roccatò, F., and Bonasoni, P.: Significant variations of trace gas
14 composition and aerosol properties at Mt. Cimone during air mass transport from North
15 Africa – contributions from wildfire emissions and mineral dust, *Atmos Chem Phys*, 9,
16 4603-4619, 2009b.

17 Cristofanelli, P., Scheel, H.-E., Steinbacher, M., Saliba, M., Azzopardi, F., Ellul, R., Fröhlich,
18 M., Tositti, L., Brattich, E., Maione, M., Calzolari, F., Duchi, R., Landi, T.C., Marinoni,
19 A., and Bonasoni, P.: Long-term surface ozone variability at Mt. Cimone WMO/GAW
20 global station (2165 m a.s.l., Italy), *Atmos Environ*, 101, 23-33, 2015.

21 Cuevas, E., Gonzalez, Y., Rodríguez, S., Guerra, J.C., Gómez-Peláez, A.J., Alonso-Pérez, S.,
22 Bustos, J., and Milford, C.: Assessment of atmospheric processes driving ozone variations
23 in the subtropical North Atlantic free troposphere, *Atmos Chem Phys*, 13, 1973-1998, 2013.

24 Daish, S.R., Dale, A.A., Dale, C.J., May, R., and Rowe, J.E.: The temporal variations of ^7Be ,
25 ^{210}Pb and ^{210}Po in England, *J Environ Radioactiv*, 84, 457-467, 2005.

- 1 Dobb, J.E., Talbot, R.W., and Gregory, G.L.: Beryllium 7 and lead 210 in the western
2 hemisphere Arctic atmosphere: Observations from three recent aircraft-based sampling
3 programs, *J Geophys Res*, 97, 16709-16715, 1992.
- 4 Dobb, J.E., Meeker, L.D., Finkel, R.C., Southon, J.R., Caffee, M.W., and Barrie, L.A.:
5 Estimation of stratospheric input to the Arctic troposphere: ^7Be and ^{10}Be in aerosols at
6 Alert, Canada, *J Geophys Res*, 99, 12855-12864, 1994.
- 7 Dobb, J.E.: Vertical mixing above Summit, Greenland: insights into seasonal and high
8 frequency variability from the radionuclide tracers ^7Be and ^{210}Pb , *Atmos Environ*, 41, 5020-
9 5030, 2007.
- 10 Dueñas, C., Fernández, M.C., Cañete, S., and Pérez, M.: ^7Be to ^{210}Pb concentration ratio in
11 ground level air in Málaga (36.7°N, 4.5°W), *Atmos Res*, 92, 49-57, 2009.
- 12 Dueñas, C., Orza, J.A.G., Cabello, M., Fernández, M.C., Cañete, S., Pérez, M., and Gordo, E.:
13 Air mass origin and its influence on radionuclide activities (^7Be and ^{210}Pb) in aerosol
14 particles at a coastal site in the western Mediterranean, *Atmos Res*, 101, 205-214, 2011.
- 15 Duncan, B.N., Strahan, S.E., and Yoshida, Y.: Model study of the cross-tropopause transport
16 of biomass burning pollution, *Atmos Chem Phys*, 7, 3713-3736, 2007.
- 17 Duncan, B.N., West, J.J., Yoshida, Y., Fiore, A.M., and Ziemke, J.R.: The influence of
18 European pollution on ozone in the Near East and northern Africa, *Atmos Chem Phys*, 8,
19 2267-2283, doi:10.5194/acp-8-2267-2008, 2008.
- 20 Feely, H.W., Larsen, R.J., and Sanderson, C.G.: Factors that cause seasonal variations in
21 beryllium-7 concentrations in surface air, *J Environ Radioactiv*, 9, 223-249, 1989.
- 22 [Feichter, J., Brost, R.A., and Heimann, M.: Three-dimensional modeling of the concentration](#)
23 [and deposition of \$^{210}\text{Pb}\$ aerosols, *J. Geophys. Res.*, 96, 22 447-22 469, 1991.](#)
- 24 Fischer, H., Kormann, R., Klüpfel, T., Gurk, C., Königstedt, R., Parchatka, U., Mühle, J., Rhee,
25 T.S., Brenninkmeijer, C.A.M., Bonasoni, P., and Stohl, A.: Ozone production and trace gas

1 correlations during the June 2000 MINATROC intensive measurement campaign at Mt.
2 Cimone. *Atmos Chem Phys*, 3, 725-738, 2003.

3 Forster, P., Ramaswamy, V., Artaxo, P., Bernsten, T., Betts, R., Fahey, D.W., Haywood, J.,
4 Lean, J., Lowe, D.C., Myhre, G., Nganga, J., Prinn, R., Raga, G., Schulz, M., and Van
5 Dorland, R.: Changes in Atmospheric Constituents and in Radiative Forcing, in *Climate*
6 *Change 2007: The Physical Science Basis. Contribution of Working Group I to the Fourth*
7 *Assessment Report of the Intergovernmental Panel on Climate Change*, [Solomon, S., Qin,
8 D., Manning, M., Chen, Z., Marquis, M., Averyt, K.B., Tignor, M., and Miller, H.L. (eds.)],
9 Cambridge University Press, Cambridge, United Kingdom and New York, NY, USA, 2007.

10 Froehlich, K., and Masarik, J.: Radionuclides as tracers and timers of processes in the
11 continental environment – Basic concepts and methodologies. In: *Radioactivity in the*
12 *Environment*, 16, Chapter 2, 27-50, *Environmental Radionuclides: Tracers and Timers of*
13 *Terrestrial Processes*. Edited by Elsevier. doi:10.1016/S1569-4860(09)01602-7, 2010

14 Gaffney, J.S, Marley, N., and Cunningham, M.M.: Natural radionuclides in fine aerosols in the
15 Pittsburgh area, *Atmos Environ*, 38, 3191-3200, 2004.

16 Gäggeler, H.W.: Radioactivity in the atmosphere, *Radiochim Acta*, 70-71, 345-353, 1995.

17 Gerasopoulos, E., Zanis, P., Stohl, A., Zerefos, C.S., Papastefanou, C., Ringer, W., Tobler, L.,
18 Hübener, S., Gäggeler, H.W., Kanter, H.J., Tositti L., and Sandrini, S.: A climatology of
19 ^7Be at four high-altitude stations at the Alps and the Northern Apennines, *Atmos Environ*,
20 35, 6347-6360, 2001.

21 Gerasopoulos, E., Zanis, P., Zerefos, C.S., Papastefanou, C., Ringer, W., Gäggeler, H.W.,
22 Tobler, L., and Kanter, H.J.: Factors and processes controlling the concentration of the
23 cosmogenic radionuclide ^7Be at high-altitude Alpine stations, In: *Radioactivity in the*
24 *Environment*, Volume 7, 863-870, Elsevier Ltd., ISSN 1569-4860, DOI10.1016/S1569-
25 4860(04)07108-6, 2005.

Deleted: ,

1 Graustein, W.C., and Turekian, K.K.: Radon fluxes from soils to the atmosphere
2 measured by ^{210}Pb - ^{226}Ra disequilibrium in soils, *Geophys Res Lett*, 17, 841-844,
3 1990.

4 Graustein, W.C., and Turekian, K.K.: ^7Be and ^{210}Pb indicate an upper troposphere source for
5 elevated ozone in the summertime subtropical free troposphere of the eastern North
6 Atlantic, *Geophys Res Lett*, 23, 539-542, 1996.

7 Hötzl, H., and Winkler, R.: Activity concentrations of ^{226}Ra , ^{228}Ra , ^{210}Pb , ^{40}K and ^7Be and their
8 temporal variations in surface air, *J Environ Radioactiv*, 5, 445-458, 1987

9 Huang M., Carmichael, G.R., Chai, T., Pierce, R.B., Oltmans, S.J., Jaffe, D.A., Bowman, K.W.,
10 Kaduwela, A., Cai, C., Spak, S.N., Weinheimer, A.J., Huey, L.G., and Diskin, G.S.:
11 Impacts of transported background pollutants on summertime western US air quality:
12 model evaluation, sensitivity analysis and data assimilation, *Atmos Chem Phys*, 13, 359-
13 391, 2013.

14 Ioannidou, A., Manolopoulou, M., and Papastefanou, C.: Temporal changes of ^7Be and ^{210}Pb
15 concentrations in surface air at temperate latitudes (40°), *Appl Radiat Isotopes*, 63(2), 277-
16 284, 2005.

17 Ioannidou, A., Vasileiadis, A., and Melas, D.: Time lag between the tropopause height and ^7Be
18 activity concentrations in surface air, *J Environ Radioactiv*, 129, 80-85, 2014.

19 Jacob, D.J., and Prather, M.J.: Radon-222 as a test of boundary layer convection in a general
20 circulation model, *Tellus B*, 42, 118-134, 1990.

21 James, P., Stohl, A., Forster, C., Eckhardt, S., Seibert, P., and Frank, A., A 15-year climatology
22 of stratosphere-troposphere exchange with a Lagrangian particle dispersion model 2. Mean
23 climate and seasonal variability, *J Geophys Res*, 108(D12), 8522,
24 doi:10.1029/2002JD002639, 2003.

- 1 Jasiulionis, R., and Wershofen, H.: A study of the vertical diffusion of the cosmogenic
2 radionuclides, ^7Be and ^{22}Na in the atmosphere. *J Environ Radioactiv*, 79, 157-169, 2005.
- 3 Johnson, W., and Viezee, W., Stratospheric ozone in the lower troposphere: i. Presentation and
4 interpretation of aircraft measurements. *Atmos Environ*, 15, 1309–1323, 1981.
- 5 Junge, C.E.: Air chemistry and radioactivity. Academic Press, New York, USA, and London,
6 UK, 382 pp, 1963.
- 7 Kinnison, D.E., Connell, P.S., Rodriguez, J.M., Rotman, D.A., Considine, D.B., Tannahill, J.,
8 Ramaroson, R., Rasch, P.J., Douglass, A.R., Baughcum, S.L., Coy, L., Waugh, D.W.,
9 Kawa, S.R., and Prather, M.J.: The Global Modeling Initiative assessment model:
10 Application to high-speed civil transport perturbation, *J Geophys Res*, 106(D2), 1693-
11 1711, 2001.
- 12 Koch, D.M., Jacob, D.J., and Graustein, W.C.: Vertical transport of tropospheric aerosols as
13 indicated by ^7Be and ^{210}Pb in a chemical tracer model, *J Geophys Res*, 101(D13), 18651-
14 18666, 1996.
- 15 Koch, D., and Rind, D.: Beryllium10/beryllium7 as a tracer of stratospheric transport, *J*
16 *Geophys Res*, 103, 3907-3917, 1998.
- 17 Kulan, A., Aldahan, A., Possnert, G., and Vintersved, I.: Distribution of ^7Be in surface air of
18 Europe, *Atmos Environ*, 40, 3855-3868, 2006.
- 19 Lal, D., Malhotra, P.K., and Peters, B.: On the production of radioisotopes in the atmosphere
20 by cosmic radiation and their application to meteorology, *J Atmos Sol-Terr Phy*, 12, 306-
21 328, 2006.
- 22 Lal, D., and Peters, B.: Cosmic ray produced radioactivity on the Earth, in: *Handbuch der*
23 *Physik*, 46/2, edited by Sitte, K., Springer-Verlag, New York, USA, pp. 551-561, 1967.
- 24 Lee, H.N., Wan, G., Zheng, X., Sanderson, C.G., Josse, B., Wang, S., Yang, W., Tang, J., and
25 Wang, C.: Measurements of ^{210}Pb and ^7Be in China and their analysis accompanied with

1 global model calculations of ^{210}Pb , *J Geophys Res*, 109, D22203,
2 doi:10.1029/2004JD005061, 2004.

3 Lee, H.N., Tositti, L., Zheng, X., and Bonasoni, P.: Analyses and comparisons of variations
4 of ^7Be , ^{210}Pb and $^7\text{Be}/^{210}\text{Pb}$ with ozone observations at two Global Atmosphere Watch
5 stations from high mountains, *J Geophys Res*, 112, D05303, doi:10.1029/2006JD007421,
6 2007

7 Lelieveld, J., Berresheim, H., Borrmann, S., Crutzen, P.J., Dentener, F.J., Fischer, H., Feichter,
8 J., Flatau, P.J., Heland, J., Holzinger, R., Kormann, R., Lawrence, M.G., Levin, Z.,
9 Markowicz, K.M., Mihopoulos, N., Minikin, A., Ramanathan, V., de Reus, M., Roelofs,
10 G.J., Scheeren, H.A., Sciare, J., Schlager, H., Schultz, M., Siegmund, P., Steil, B.,
11 Stephanou, E.G., Stier, P., Traub, M., Warneke, C., Williams, J., and Ziereis, H.: Global
12 air pollution crossroads over the Mediterranean. *Science*, 298, 794-799, 2002.

13 Li, Q., Jacob, D.J., Logan, J.A., Bey, I., Yantosca, R.M., Liu, H., Martin, R.V., Fiore, A.M.,
14 Field, B.D., Duncan, B.N.: A Tropospheric Ozone Maximum Over the Middle East,
15 *Geophys Res Lett*, 28(17), 3235-3238, 2001.

16 Likuku, A.S.: Factors influencing ambient concentrations of ^{210}Pb and ^7Be over the city of
17 Edinburgh (55.9°N, 03.2°W), *J Environ Radioactiv*, 87, 289-304, 2006.

18 Liu, H., Jacob, D.J., Bey, I., and Yantosca, R.M.: Constraints from the ^{210}Pb and ^7Be on wet
19 deposition and transport in a global three-dimensional chemical tracer model driven by
20 assimilated meteorological fields, *J Geophys Res*, 106, D11, 12109-12128, 2001.

21 Liu, H., Jacob, D.J., Dibb, J.E., Fiore, A.M., and Yantosca, R.M.: Constraints on the sources
22 of tropospheric ozone from ^{210}Pb - ^7Be - O_3 correlations, *J Geophys Res*, 109(D07306),
23 doi:10.1029/2003JD003988, 2004.

24 Liu, H., Considine, D. B., Horowitz, L. W., Crawford, J. H., Rodriguez, J. M., Strahan, S. E.,
25 Damon, M. R., Steenrod, S. D., Xu, X., Kouatchou, J., Carouge, C., and Yantosca, R. M.:

- 1 Using beryllium-7 to assess cross-tropopause transport in global models, *Atmos. Chem.*
2 *Phys.*, 16, 4641-4659, doi:10.5194/acp-16-4641-2016, 2016.
- 3 Lozano, R.L., Hernández-Ceballos, M.A., San Miguel, E.G., Adame, J.A., and Bolívar, J.P.:
4 Meteorological factors influencing the ^7Be and ^{210}Pb concentrations in surface air from the
5 southwestern Iberian Peninsula, *Atmos Environ*, 63, 168-178, 2012.
- 6 Lozano, R.L., Hernández-Ceballos, M.A., Rodrigo, J.F., San Miguel, E.G., Casas-Ruiz, M.,
7 García-Tenorio, R., and Bolívar, J.P.: Mesoscale behavior of ^7Be and ^{210}Pb in superficial
8 air along the Gulf of Cadiz (south of Iberian peninsula), *Atmos Environ*, 80, 75-84, 2013.
- 9 Marinoni, A., Cristofanelli, P., Calzolari, F., Roccatò, F., Bonafé, U., and Bonasoni, P.:
10 Continuous measurements of aerosol physical parameters at the Mt. Cimone GAW Station
11 (2165 m asl, Italy), *Sci Total Environ*, 391, 241-251, 2008.
- 12 Millàn, M., Sanz, J., Salvador, R., and Mantilla, E.: Atmospheric dynamics and ozone cycles
13 related to nitrogen deposition in the western Mediterranean, *Environ Pollut*, 118, 167-186,
14 2006.
- 15 Monks, P.S., Granier, C., Fuzzi, S., Stohl, A., Williams, M.L., Akimoto, H., Amann, M.,
16 Baklanov, A., Baltensperger, U., Bey, I., Blake, N., Blake, R.S., Carslaw, K., Cooper, O.R.,
17 Dentener, F., Fowler, D., Fragkou, E., Frost, G.J., Generoso, S., Ginoux, P., Grewe, V.,
18 Guenther, A., Hansson, H.C., Henne, S., Hjorth, J., Hofzumahaus, A., Huntrieser, H.,
19 Isaksen, I.S.A., Jenkin, M.E., Kaiser, J., Kanakidou, M., Klimont, Z., Kulmala, M., Laj, P.,
20 Lawrence, M.G., Lee, J.D., and Liousse, C.: Atmospheric composition change – global and
21 regional air quality, *Atmos Environ*, 43, 5268-5350, 2009.
- 22 Moore, H.E., Poet, S.E., and Martell, E.A.: ^{222}Rn , ^{210}Pb , ^{210}Bi , and ^{210}Po , profiles and aerosol
23 residence times versus altitude, *J Geophys Res*, 78, 7065-7075, 1973.
- 24 Nazaroff, W.W.: Radon transport from soil to air, *Rev Geophys*, 30, 137-160, 1992.

Deleted: .

- 1 ORTEC: Gamma-Vision 32 A66-B32 user's manual. ORTEC USA, Part No. 783620, Manual
2 Revision D, 2003.
- 3 Papastefanou, C., and Ioannidou, A.: Aerodynamic size association of ^7Be in ambient aerosols.
4 *J Environ Radioactiv*, 26, 273-282, 1995.
- 5 Pham, M.K., Betti, M., Nies ,H., and Povinec, P.P.: Temporal changes of ^7Be , ^{137}Cs and ^{210}Pb
6 activity concentrations in surface air at Monaco and their correlation with meteorological
7 parameters, *J Environ Radioactiv*, 102, 1045-1054, 2011.
- 8 Rastogi, N., and Sarin, M.M.: Atmospheric ^{210}Pb and ^7Be in ambient aerosols over low- and
9 high-altitude sites in 34 semiarid region: Temporal variability and transport processes, *J*
10 *Geophys Res*, 113, doi:10.1029/2007JD009298, 2008.
- 11 Rehfeld, S., and Heimann, M.: Three dimensional atmospheric transport simulation of the
12 radioactive tracers ^{210}Pb , ^7Be , ^{10}Be , and ^{90}Sr , *J Geophys Res*, 100 (D12), 26141-26161,
13 1995.
- 14 Reiter, E.R.: Weather phenomena of the Mediterranean basin. Part 1. General description of
15 the meteorological processes, In: Handbook for forecasters in the Mediterranean basin,
16 Environment Prediction Research Facility, Naval Postgraduate School, Monterey,
17 California, U.S. Department of Commerce, available at [http://www.dtic.mil/cgi-](http://www.dtic.mil/cgi-bin/GetTRDoc?AD=ADA024271)
18 [bin/GetTRDoc?AD=ADA024271](http://www.dtic.mil/cgi-bin/GetTRDoc?AD=ADA024271), last accessed 15 March 2016, 1975.
- 19 Reiter, R., Sladkovich, K., Pötzl, K., Carnuth, W., and Kanter H.J.: Studies on the influx of
20 stratospheric air into the lower troposphere using cosmic-ray produced radionuclides and
21 fallout, *Arch Meteor Geophy A*, Vol.20(3), 211-246, 1971.
- 22 Reiter, R., Munzert, K., Kanter, H.-J., and Pötzl, K.: Cosmogenic radionuclides and ozone at a
23 mountain station at 3.0 km a.s.l., *Arch Meteor Geophy B*, 32, 131-160, 1983.
- 24 Rienecker, M.M., Suarez, M.J., Gelaro, R., Todling, R., Bacmeister, J., Liu, E., Bosilovich,
25 M.G., Schubert, S.D., Takacs, L., Kim, G.-K., Bloom, S., Chen, J., Collins, D., Conaty, A.,

1 da Silva, A., Gu, W., Joiner, J., Koster, R.D., Lucchesi, R., Molod, A., Owens, T., Pawson,
2 S., Pegion, P., Redder, C.R., Reichle, R., Robertson, F.R., Ruddick, A.G., Sienkewicz, M.,
3 and Woollen, J.: MERRA: NASA's Modern-Era Retrospective Analysis for Research and
4 Applications. *J Climate*, 24(14), 3624-3648, 2011.

5 Rodriguez, J.M., Logan, J.A., Bergmann, D., Megretskaja, I., Jacob, D.J., Xie, H., Das, B., and
6 Strahan, S.E.: The impact of meteorological fields on tropospheric ozone distributions
7 calculated by the Global Modeling Initiative (GMI) chemical-transport model, in:
8 Quadrennial Ozone Symposium QOS 2004, edited by: Zerefos, C., pp.147, International
9 Ozone Commission, Kos, Greece, 2004

10 Rotman, D.A., Tannahill, J.R., Kinnison, D.E., Connell, P.S., Bergmann, D., Proctor, D.,
11 Rodriguez, J.M., Lin, S.J., Rood, R.B., Prather, M.J., Rasch, P.J., Considine, D.B.,
12 Ramarosan, R., and Kawa, S.R.: Global Modeling Initiative assessment model: Model
13 description, integration, and testing of the transport shell, *J Geophys Res*, 106(D2), 1669-
14 1691, 2001.

15 Schery, S.D., Whittlestone, S., Hart, K.P., and Hill, S.E.: The flux of radon and thoron from
16 Australian soils, *J Geophys Res*, 100, 26141-26161, 1989.

17 SILSO (Sunspot Index and Long-term Solar Observation), World Data Center – Sunspot
18 Number and Long-Term Solar Observations, Royal Observatory of Belgium, on-line
19 Sunspot Number catalogue, available at <http://sidc.oma.be/silso/>, last accessed 15 March
20 2016

21 Simon, J., Meresova, J., Sykora, I., Jeskovsky, M., and Holy, K.: Modeling of temporal
22 variations of vertical concentration profile of ^7Be in the atmosphere. *Atmos Environ*, 43,
23 2000-2004, 2009.

24 Steinmann, P., Zeller, M., Beuret, P., Ferreri, G., and Estier, S.: Cosmogenic ^7Be and ^{22}Na in
25 ground level air in Switzerland (1994-2011), *J Environ Radioactiv*, 124, 68-73, 2013.

1 Stohl, A., Wernli, H., James, P., Borqui, M., Forster, C., Liniger, M.A., Seibert, P., and
2 Sprenger, M.: A new perspective of stratosphere-troposphere exchange, *Bull Am Meteor*
3 *Soc*, 84, 1565-1573 DOI: 10.1175/BAMS-84-11-1565, 2003.

4 Strahan, S.E., Duncan, B.N., and Hoor, P.: Observationally-derived diagnostics of transport in
5 the lowermost stratosphere and their application to the GMI chemistry transport model.
6 *Atmos Chem Phys*, 7, 1435-2445, 2007

7 Todorovic, D., Popovic, D., Djuric, G., Radenkovic, M.: ^7Be to ^{210}Pb concentration ratio in
8 ground level air in Belgrade area, *J Environ Radioactiv*, 79, 297-307, 2005.

9 Tositti, L., Riccio, A., Sandrini, S., Brattich, E., Baldacci, D., Parmeggiani, S., Cristofanelli,
10 P., and Bonasoni, P.: Short-term climatology of PM10 at a high altitude background station
11 in southern Europe, *Atmos Environ*, 65, 145-152, 2013.

12 Tositti, L., Brattich, E., Cinelli, G., and Baldacci, D.: 12 years of ^7Be and ^{210}Pb data in Mt.
13 Cimone, and their correlation with meteorological parameters, *Atmos Environ*, 87C, 108-
14 122. doi: 10.1016/j.atmosenv.2014.01.014, 2014.

15 Trickl, T., Feldmann, H., Kanter, H.-J., Scheel, H.-E., Sprenger, M., Stohl, A. and Wernli, H.,
16 2010. Forecasted deep stratospheric intrusions over central Europe: case studies and
17 climatologies, *Atmos Chem Phys*, 10, 499-524.

18 Trigo, I.F., Bigg, G.R., and Davies, T.D.: Climatology of cyclogenesis mechanisms in the
19 Mediterranean. *Mon Weather Rev*, 130, 549-569, 2002.

20 Turekian, K.K., Nozaki, Y., and Benninger, L.K.: Geochemistry of atmospheric radon and
21 radon products. *Annu Rev Earth Pl Sc*, 5, 227-255, 1977.

22 Turekian, K.K., and Graustein, W.C.: Natural Radionuclides in the Atmosphere, in: *Treatise*
23 *on Geochemistry*, Volume 4, Ralph Keeling, F. (Ed.), Holland, H.D., and Turekian, K.K.
24 (executive editors), pp. 347, doi:10.1016/B0-08-043751-6/04042-1, ISBN 0-08-043751-6.
25 Elsevier, p.261-279, 2003.

Formatted: Font: (Default) Times New Roman

1 Usoskin, I., and Kovaltsov, G.: Production of cosmogenic ^7Be isotope in the atmosphere: full
2 3D modelling. *J Geophys Res*, 113, D12107, 2008.

3 van Dingenen, R., Putaud, J.P., Martins-Dos Santos, S., Raes, F. Physical aerosol properties
4 and their relation to air mass origin at Monte Cimone (Italy) during the first MINATROC
5 campaign, *Atmos Chem Phys*, 5, 2203-2226, 2005.

6 Viezee, W., and Singh, H.B.: The distribution of beryllium-7 in the troposphere. Implications
7 on stratosphere/tropospheric air exchange, *Geophys Res Lett*, 7, 805-808, 1980.

8 Wilkening, M.H., Clements, W.E., and Stanley, D.: Radon222 flux measurements in widely
9 separated regions, In: *The Natural Radiation Environment II*, pp. 717-730, U.S. Energy and
10 Res. Dev. Admin., Oak Ridge, Tenn, USA, 1975.

11 Winkler, R., Dietl, F., Frank, G., and Thiersch, J.: Temporal variation of ^7Be and ^{210}Pb size
12 distributions in ambient aerosols, *Atmos Environ*, 32, 983-991, 1998.

13 WMO-GAW (World Meteorological Organization - Global Atmosphere Watch): 1st
14 International Expert Meeting on Sources and Measurements of Natural Radionuclides
15 Applied to Climate and Air Quality Studies, (Gif-sur-Yvette, France, 3-5 June 2003) (WMO
16 TD No. 1201), Report No. 155 [available at
17 <ftp://ftp.wmo.int/Documents/PublicWeb/arep/gaw/gaw155.pdf>, last accessed 15 March
18 2016], 2004

19 Zanis, P., Schuepbach, E., Gäggeler, H.W., Huebener, S., and Tobler, L.: Factors controlling
20 Beryllium-7 at Jungfrauoch in Switzerland, *Tellus*, 51 (4), 789-805, 1999.

21 Zanis, P., Monks, P.S., Schuepbach, R., Carpenter, L.J., Green, T.J., Mills, G.P, Bauguitte, S.,
22 and Penkett, S.A.: In situ ozone production under free tropospheric conditions during
23 FREETEX '98 in the Swiss Alps, *J Geophys Res*, 105 (D1), 24223-24234, 2000.

24 Zanis, P., Gerasopoulos, E., Priller, A., Schnabel, C., Stohl, A., Zerefos, C., Gäggeler, H.W.,
25 Tobler, L., Kubik, P.W., Kanter, H.J., Scheel, H.E., Luterbacher, J., and Berger, M.: An

1 estimate of the impact of stratosphere-to-troposphere transport (STT) on the lower free
2 tropospheric ozone over the Alps using ^{10}Be and ^7Be measurements, J Geophys Res,
3 108(D12), 8520, doi:10.1029/2002JD002604, 2003.

4

5

6

7

8

9

10

11

12

13

14

15

16

17

18

19

20

21

22

23

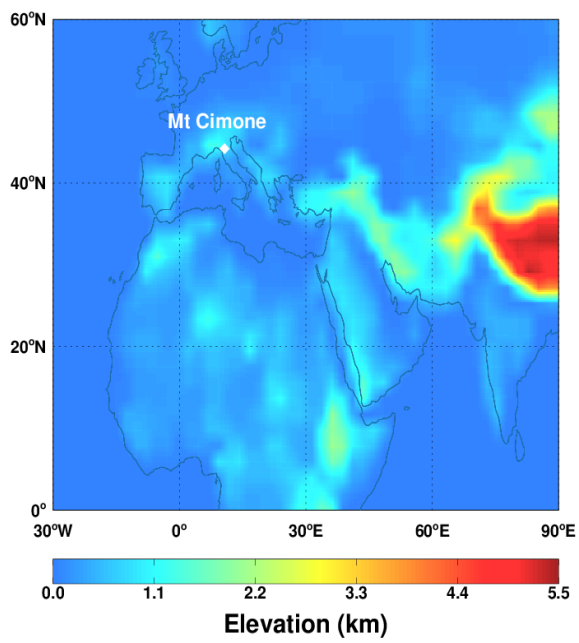
24

25

1

2

3 **Figures**



4

5 **Figure 1.** Surface elevations (km) in the model. The white dot indicates the location of Mt.

6 Cimone (44°12' N, 10°42' E, 2165 m asl).

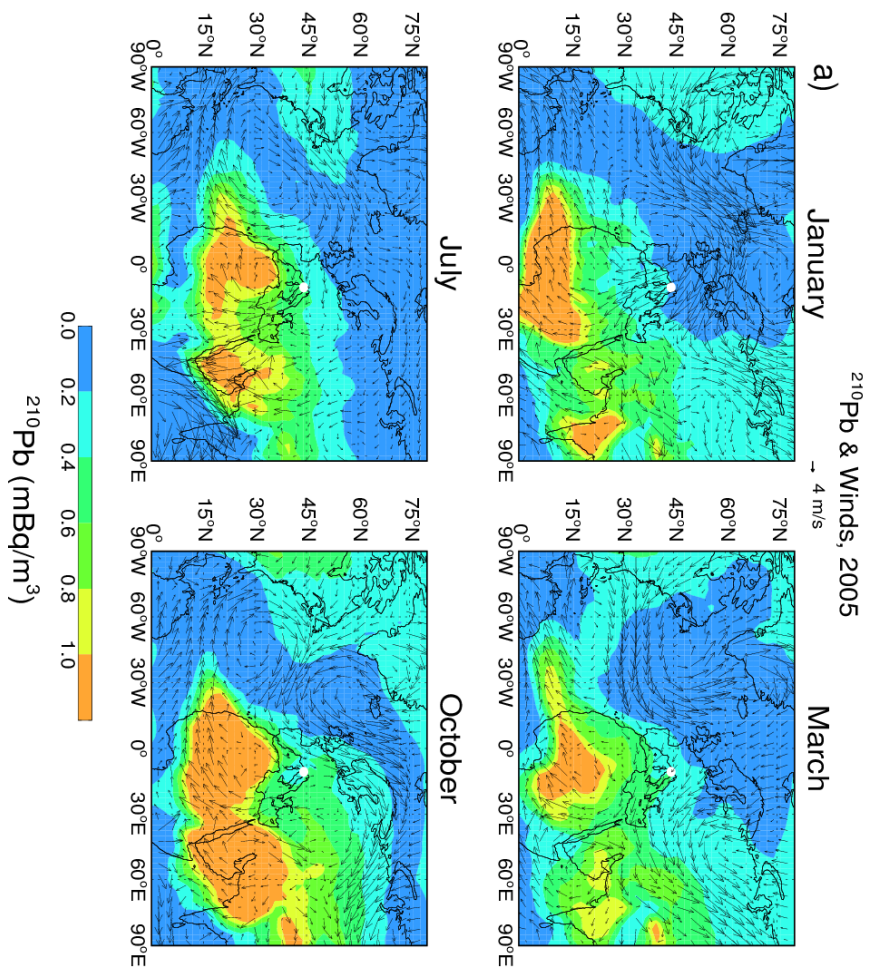
7

8

9

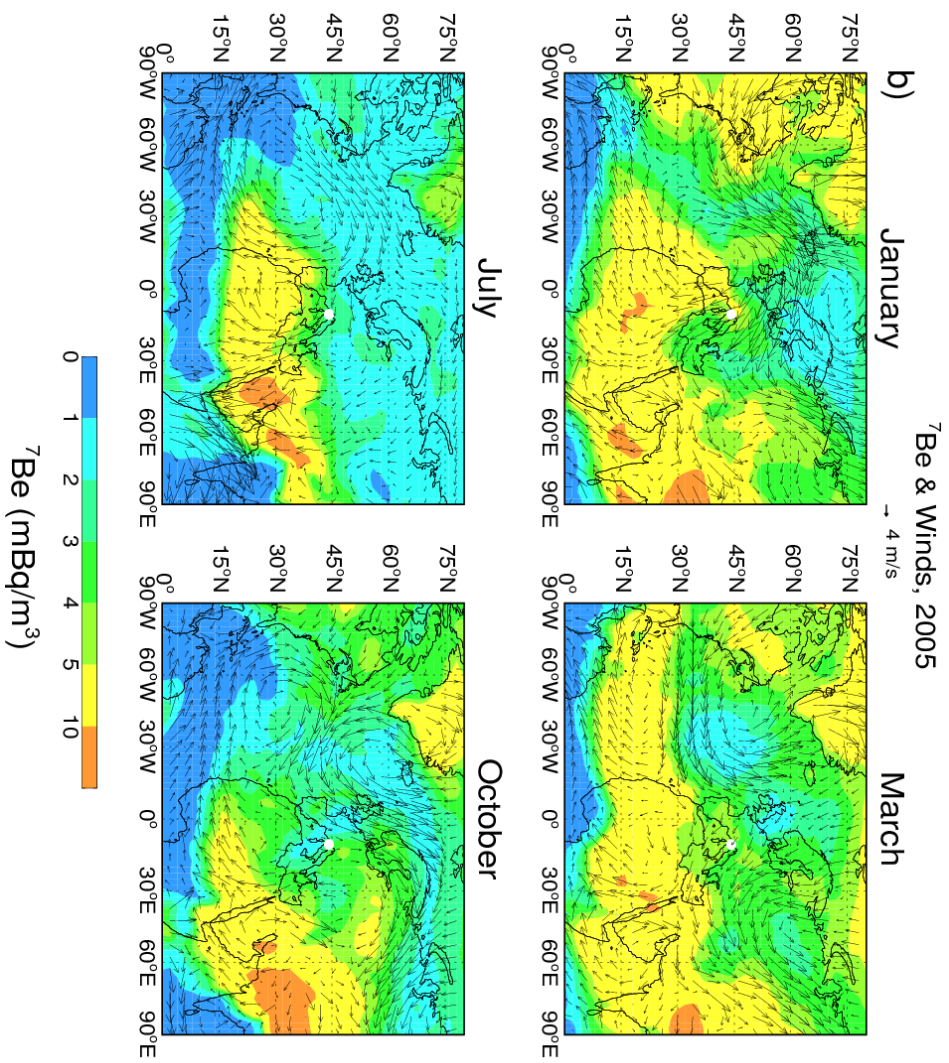
10

11



1

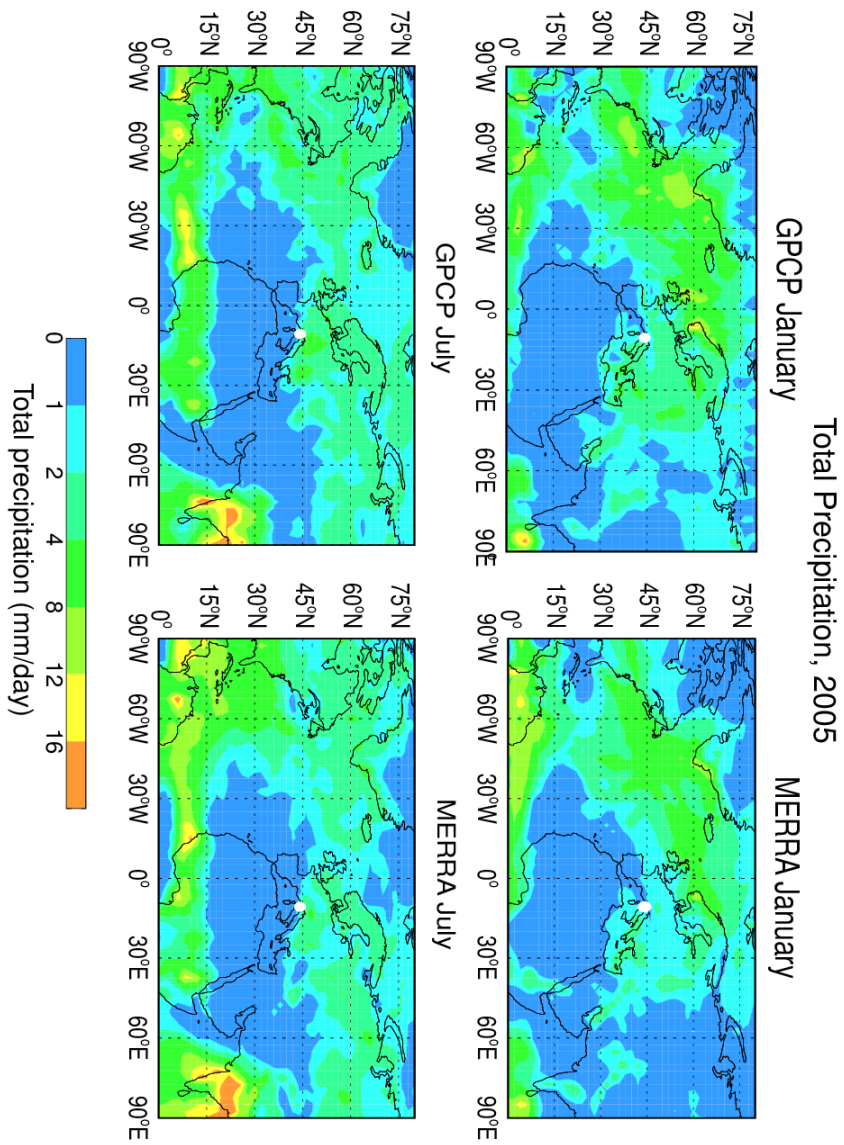
2 **Figure 2.** Simulated monthly mean (a) ²¹⁰Pb concentrations and (b) ⁷Be concentrations, at the
 3 elevation of Mt. Cimone. Arrows represent the seasonality of winds in the MERRA
 4 meteorological data. The white dot indicates the location of Mt. Cimone (44°12' N, 10°42' E,
 5 2165 m asl). To be continued.



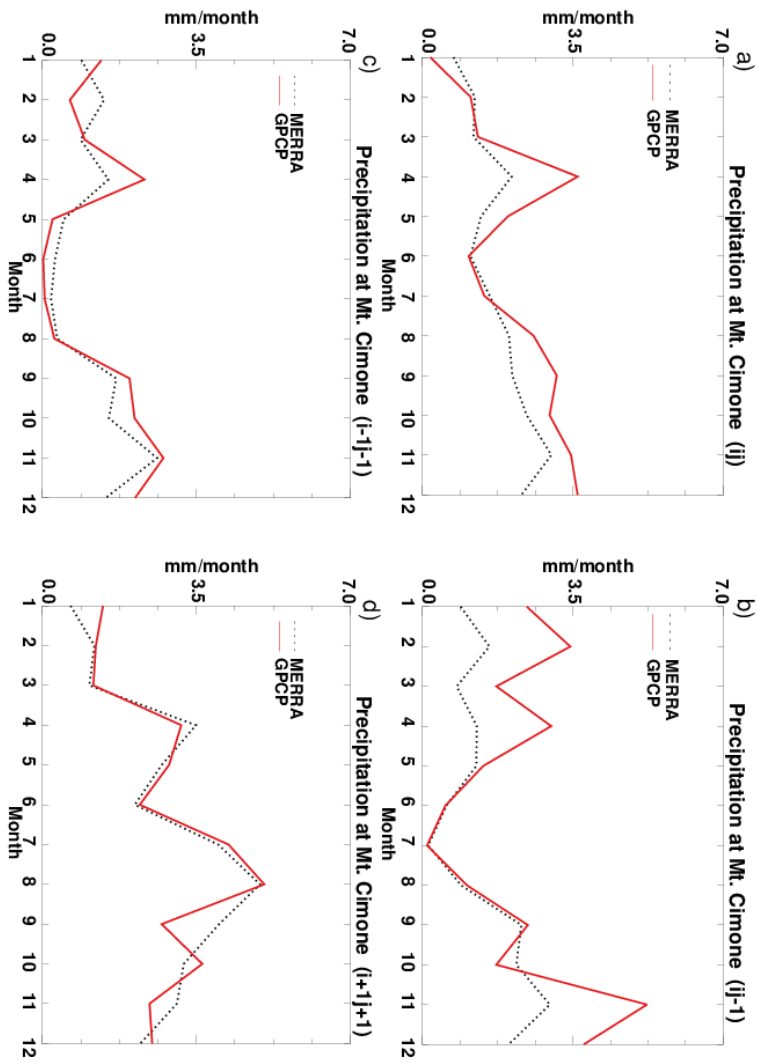
1

2 **Figure 2.** (continued)

3

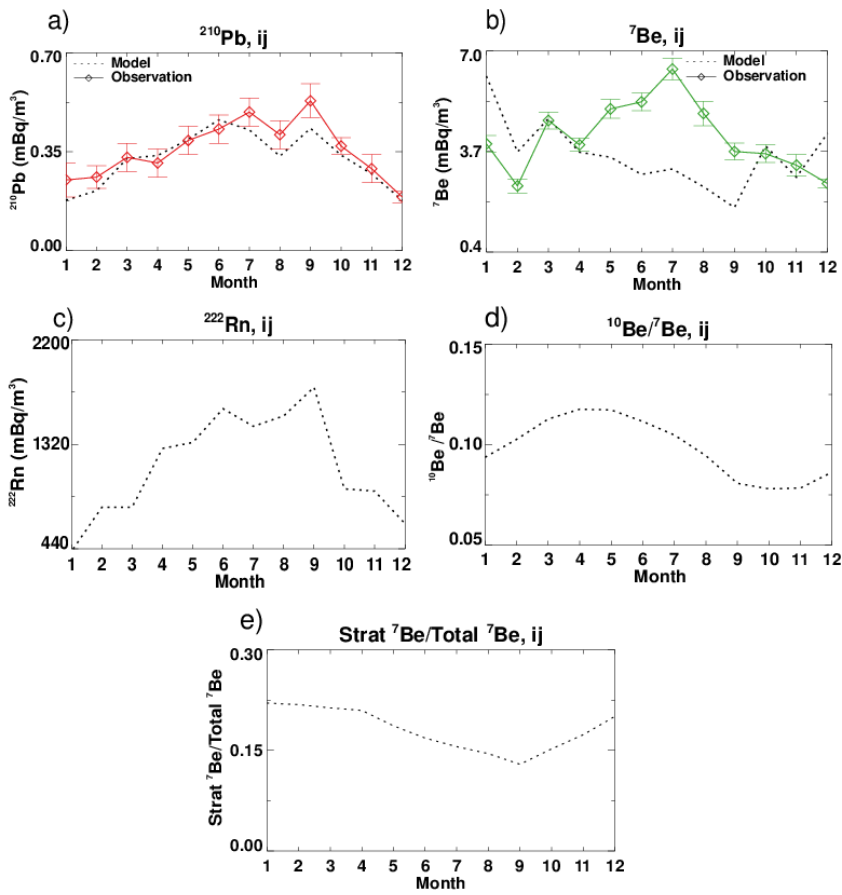


1
 2 **Figure 3.** Comparison of the MERRA total precipitation (0-75°N, 90°W-90°E) during January
 3 and July 2005 with that in the GPCP observations. The white dot indicates the location of Mt.
 4 Cimone (44°12'N, 10°42'E, 2165 m asl).



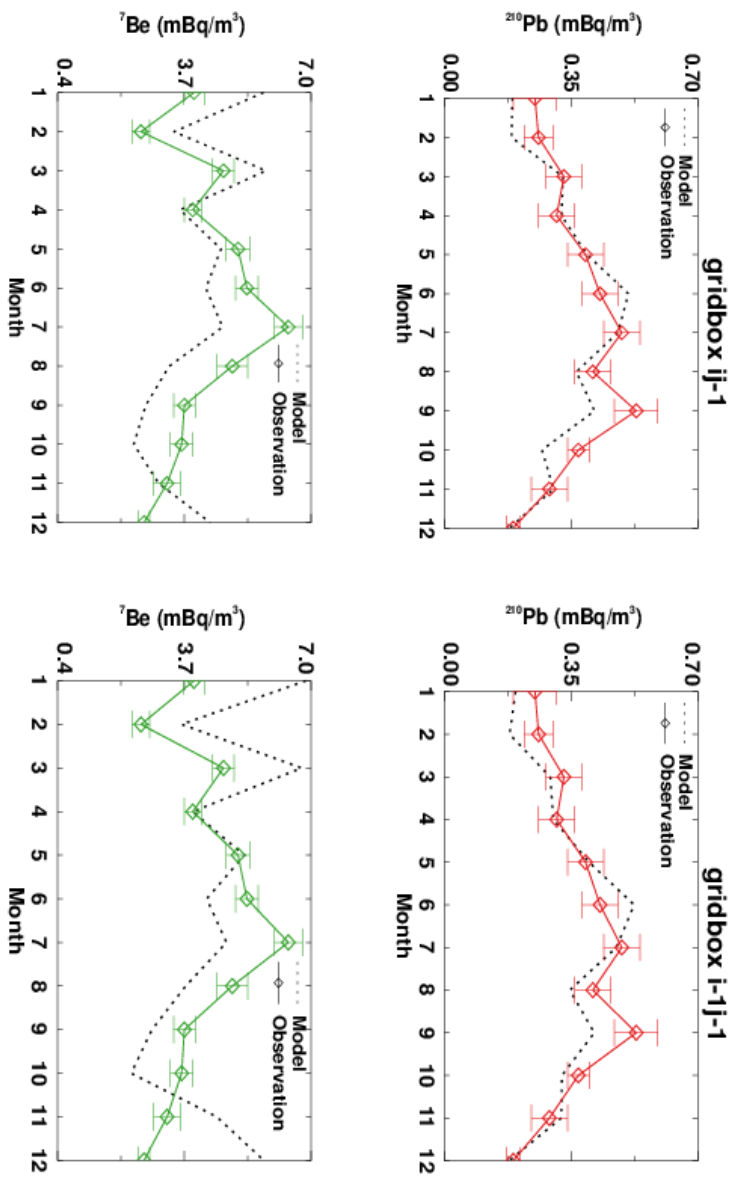
1

2 **Figure 4.** Comparison of the seasonal precipitation at Mt. Cimone in the MERRA
 3 meteorological data set with that in the GPCP observations for (a) the model gridbox (“ij”)
 4 corresponding to the location of Mt. Cimone, (b) the model gridbox (“i-1j”) to the west of “ij”,
 5 (c) the model gridbox (“i-1j-1”) to the southwest of “ij”, and (d) the model gridbox (“i+1j+1”)
 6 to the northeast of “ij”.



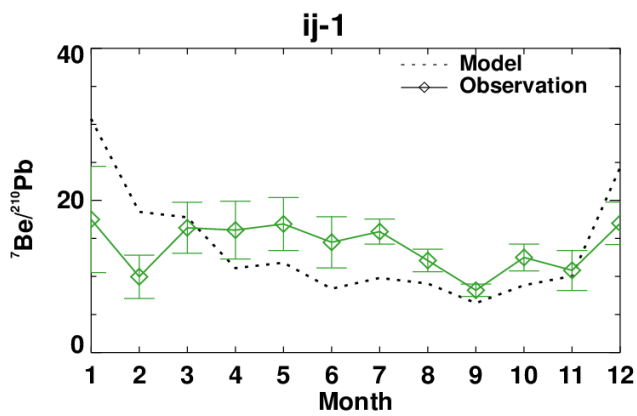
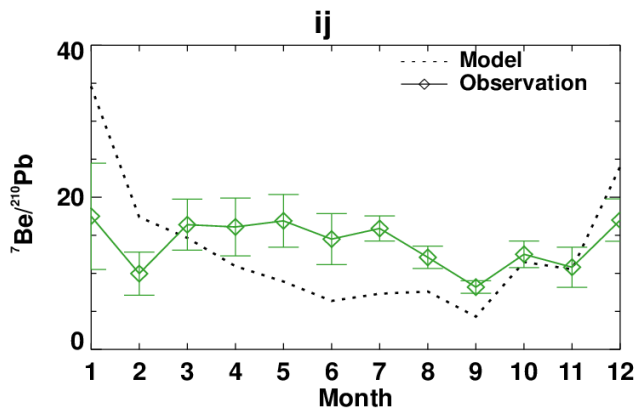
1

2 **Figure 5 (a,b,c,d,e).** Comparison of GMI simulated (black dotted line) monthly (a) ^{210}Pb and
 3 (b) ^7Be activities with those observed at Mt. Cimone (solid lines) in 2005. Also shown are GMI
 4 simulated monthly activities of (c) ^{222}Rn , (d) $^{10}\text{Be}/^7\text{Be}$ ratios, and (e) strat $^7\text{Be}/\text{total } ^7\text{Be}$ ratios.
 5 Model values are for the “ij” gridbox corresponding to the location of Mt. Cimone. Vertical
 6 bars indicate the uncertainty in observed activities.



1

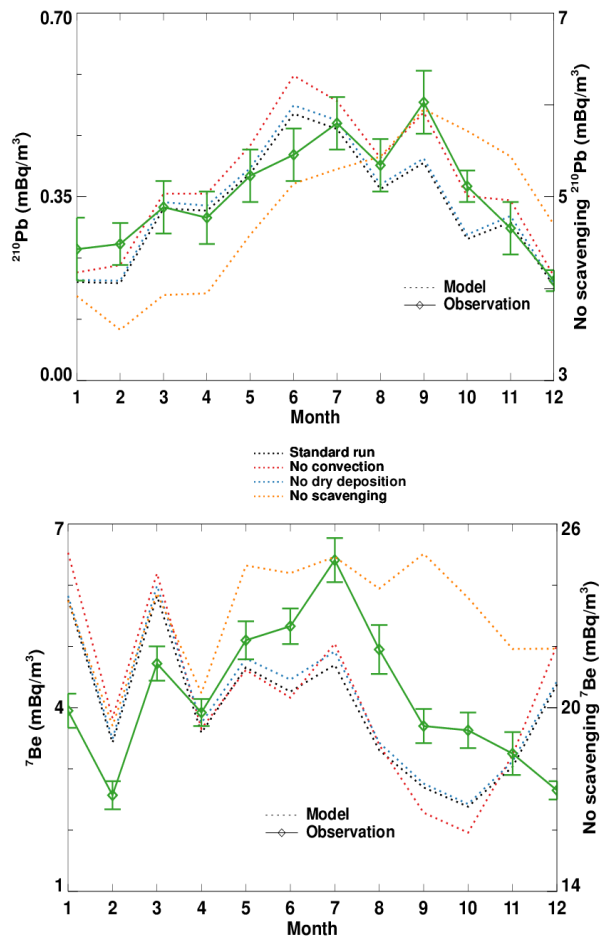
2 **Figure 6.** Same as Figure 5(ab), but for the “ij-1” to the south of “ij” (left column) and “i-1j-
 3 1” to the southwest of “ij” (right column) grids, respectively.



1

2 **Figure 7.** Comparison between GMI simulated monthly ${}^7\text{Be}/{}^{210}\text{Pb}$ ratios at the “ij” and “ij-1”
 3 grids (black dotted line) and those from the observations at Mt. Cimone (green solid line).
 4 Vertical bars indicate the uncertainty in observed activities.

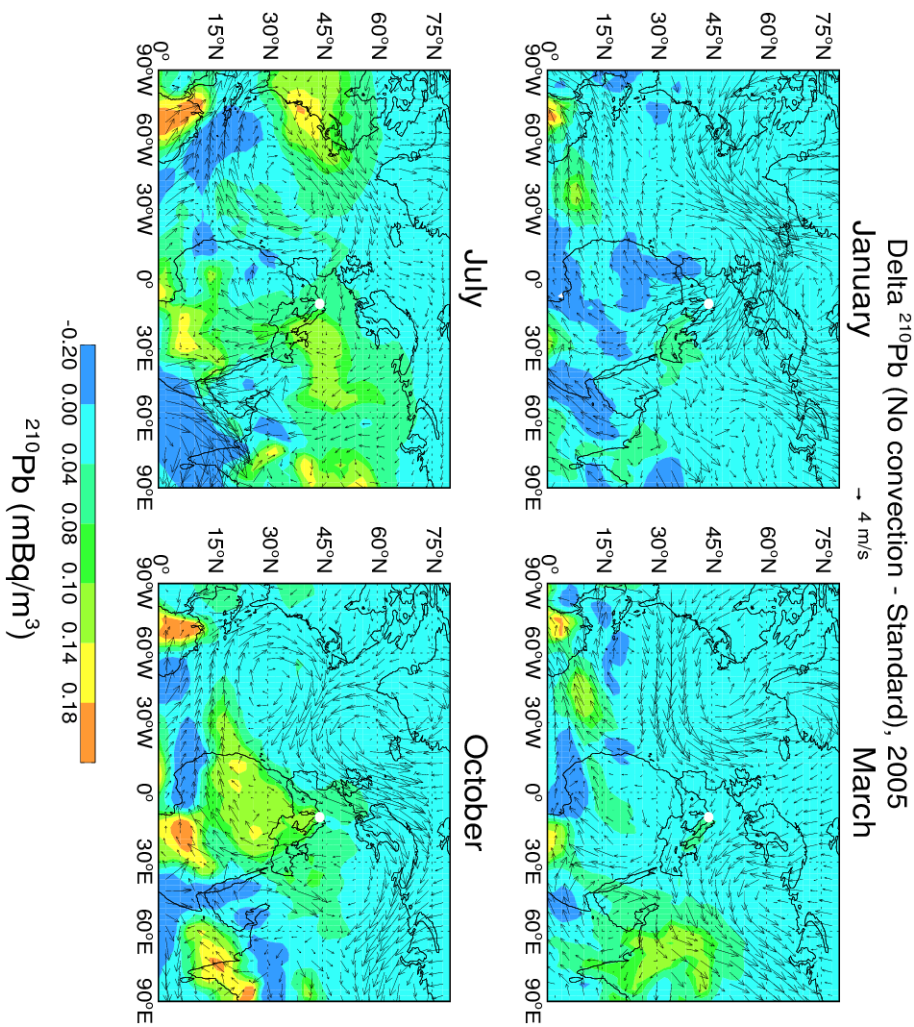
5



1

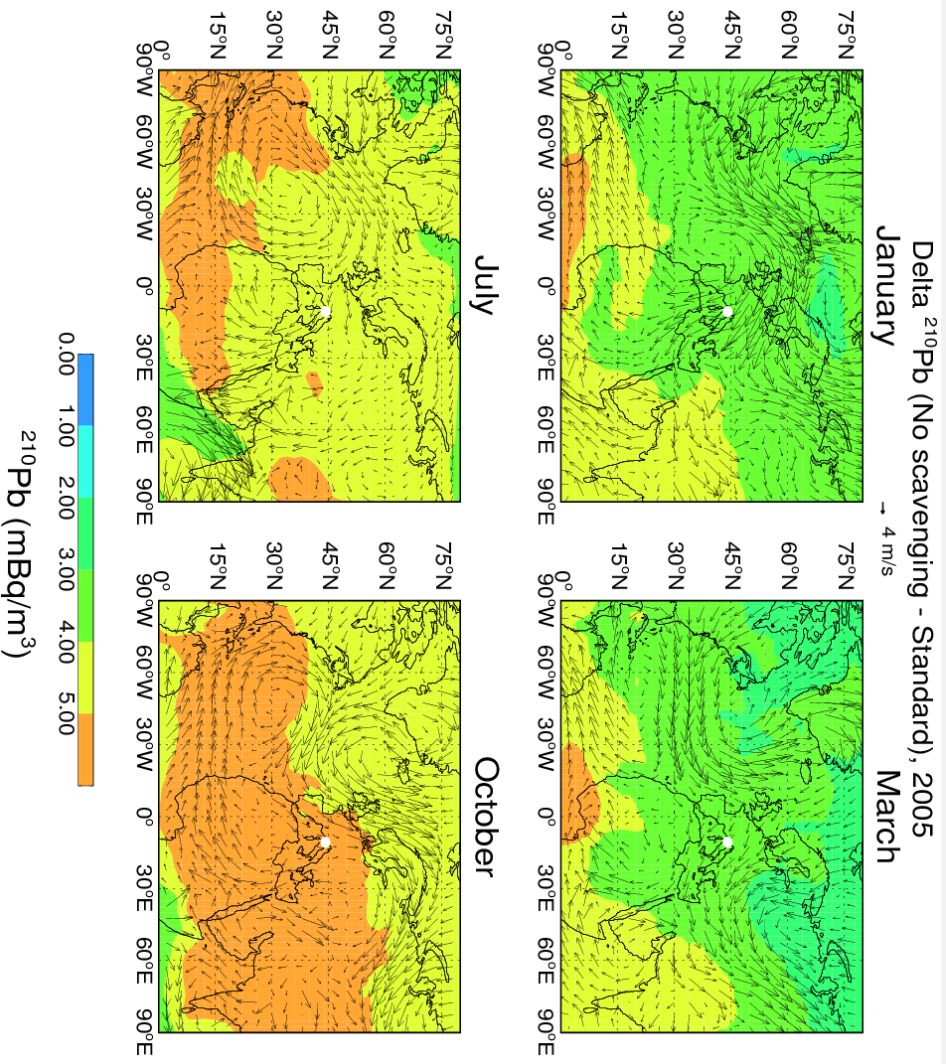
2 **Figure 8.** Comparison of GMI simulated monthly ^{210}Pb and ^7Be activities at Mt. Cimone
 3 between the standard (black dotted line) and the sensitivity runs (“ij-1” grid). The sensitivity
 4 runs are those without convective transport/scavenging (red dotted line), without dry deposition
 5 (blue dotted line), and without scavenging (orange dotted line; y-axis on the right). The
 6 observations are shown as green solid line. Vertical bars indicate the uncertainty in observed
 7 activities.

1



2

3 **Figure 9.** GMI simulated differences of ^{210}Pb concentrations at the elevation of Mt. Cimone
4 between a sensitivity run without convection (i.e., without transport and scavenging in
5 convective updrafts) and the standard run. Arrows denote MERRA winds. The white dot
6 indicates the location of Mt. Cimone (44°12' N, 10°42' E, 2165 m asl).



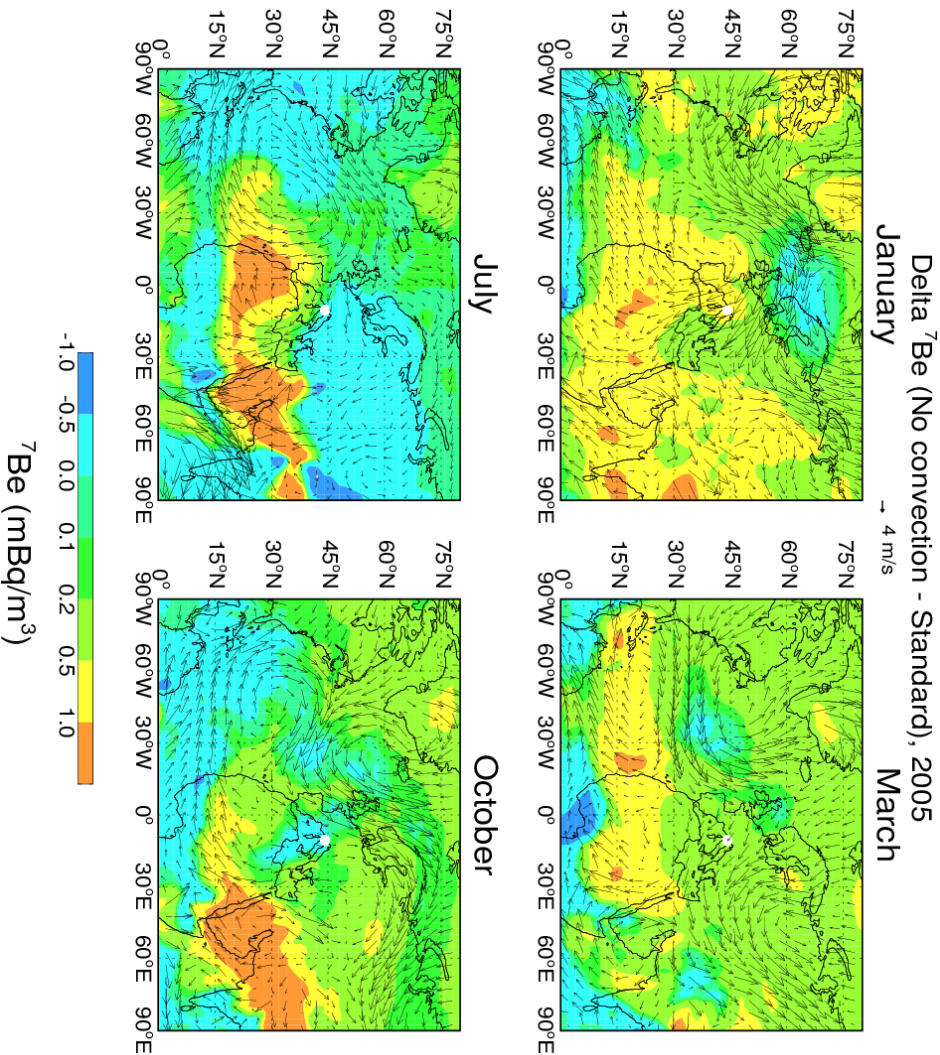
1

2 **Figure 10.** Same as Figure 9, but for a sensitivity simulation where wet scavenging is turned

3 off.

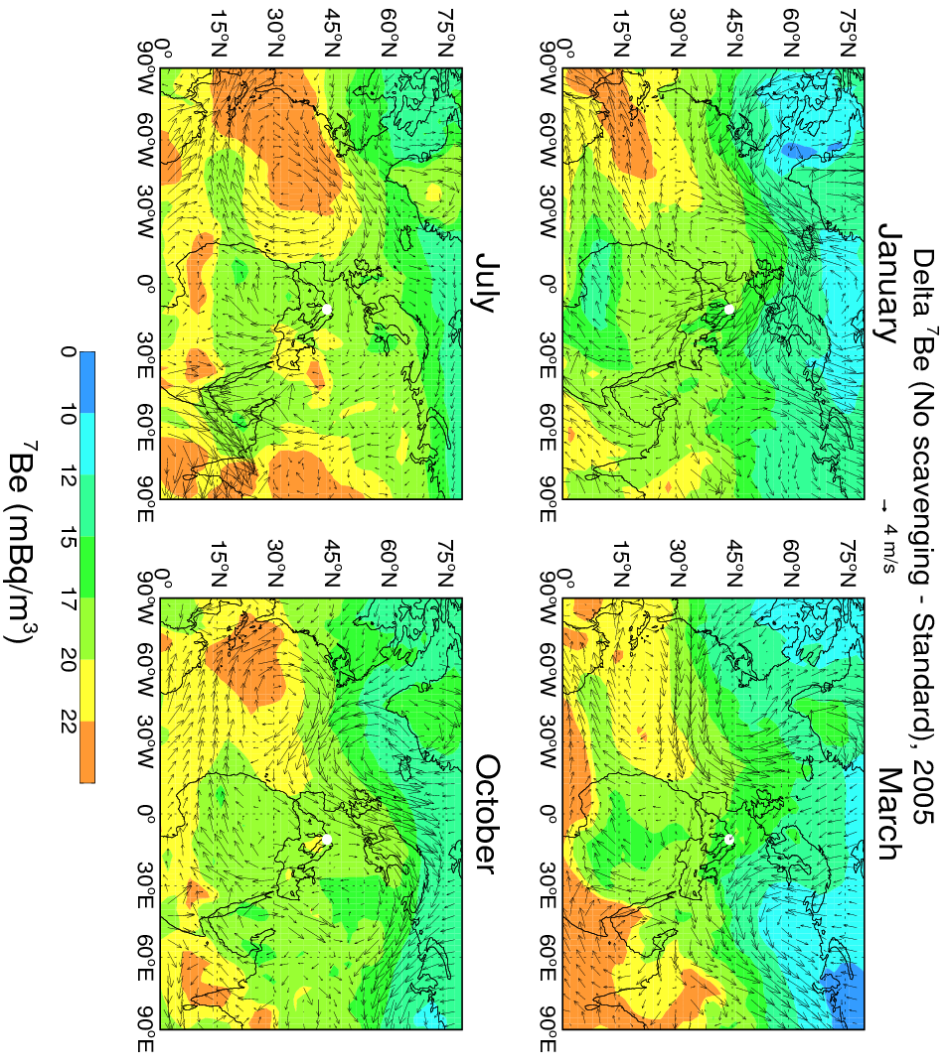
4

5



1 **Figure 11.** GMI simulated differences of ⁷Be concentrations at the elevation of Mt. Cimone
 2 between a sensitivity run without convection and the standard run. Arrows denote MERRA
 3 winds. The white dot indicates the location of Mt. Cimone (44°12' N, 10°42' E, 2165 m asl).

4



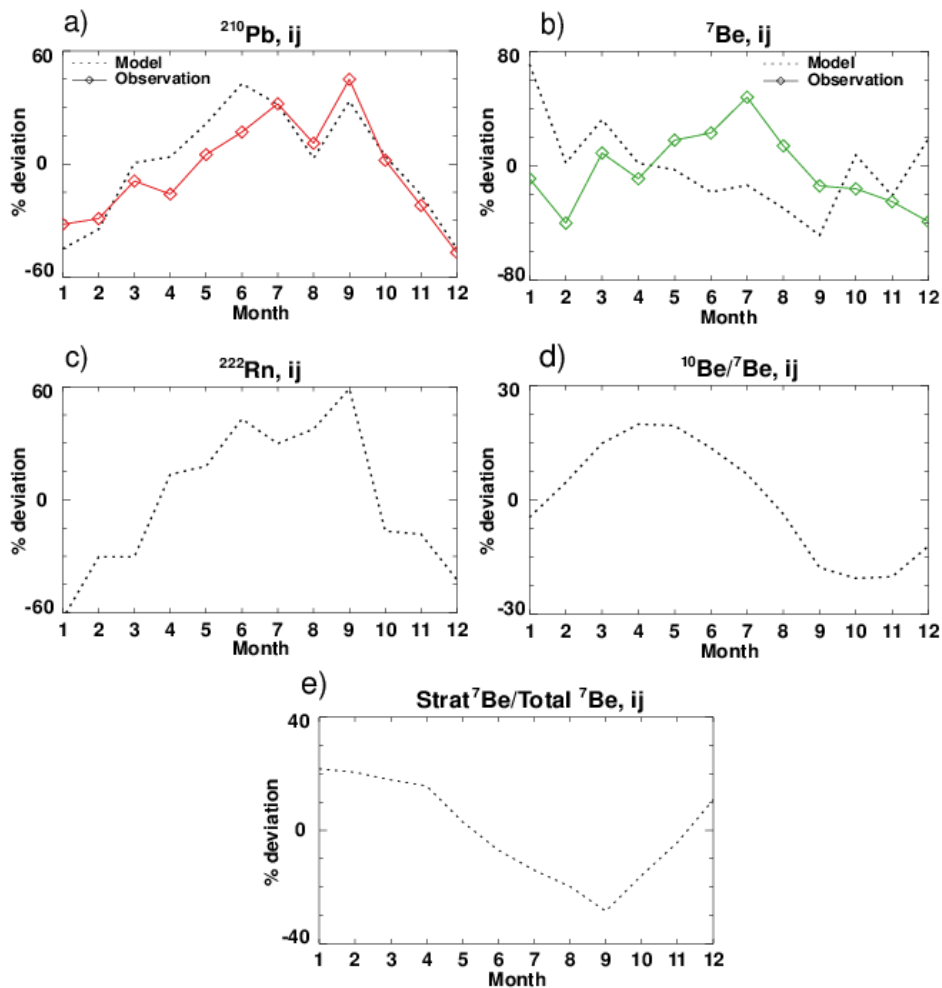
1

2 **Figure 12.** Same as Figure 11 but for the difference between a sensitivity run without wet
 3 scavenging and the standard run.

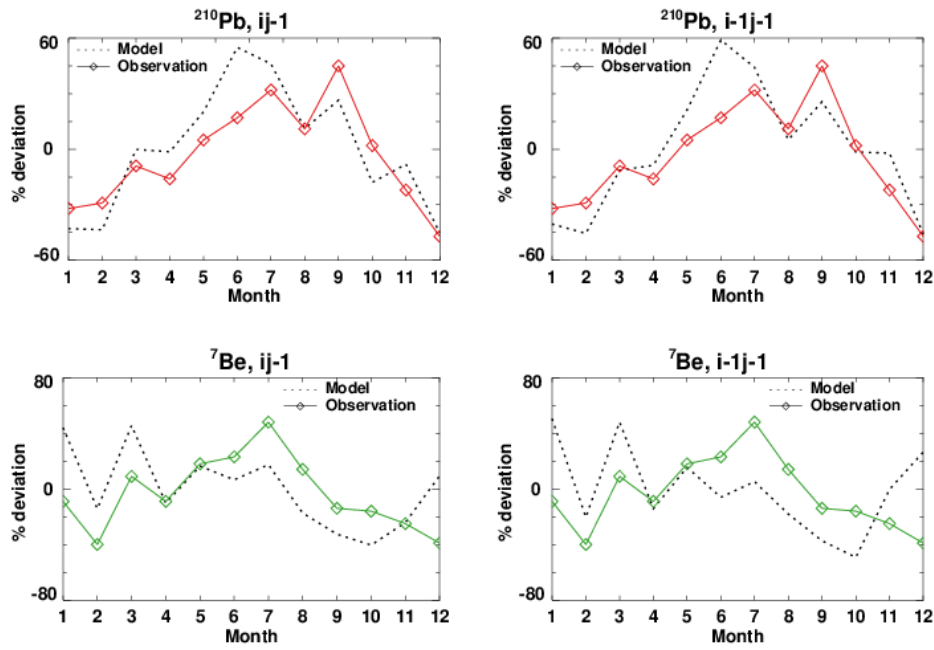
4

5

1 Supplementary Material



2
 3 **SI Figure 1 (a,b,c,d,e).** Comparison of GMI simulated (black dotted line) percentage
 4 deviations from the annual means of (a) ^{210}Pb and (b) ^7Be concentrations with those observed
 5 at Mt. Cimone (solid lines). Model values are for the “ij” gridbox corresponding to the location
 6 of Mt. Cimone. Also shown are GMI simulated monthly fluctuations of (c) ^{222}Rn activities, (d)
 7 $^{10}\text{Be}/^7\text{Be}$ ratios and (e) strat $^7\text{Be}/\text{total } ^7\text{Be}$ ratios.



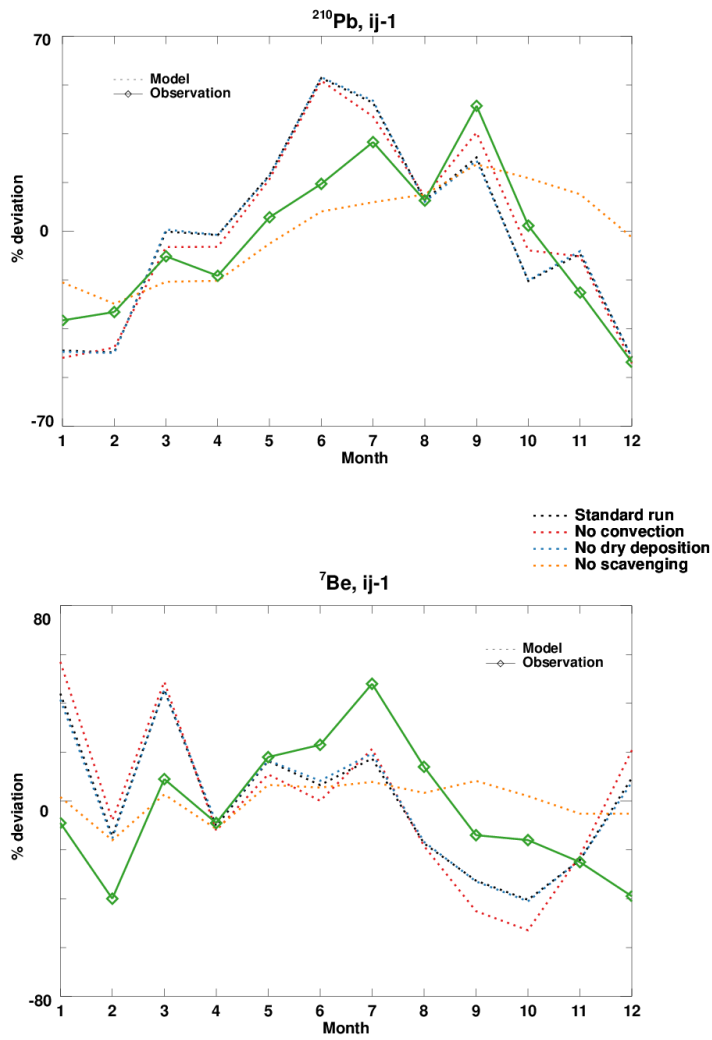
1

2 **SI Figure 2.** Same as SI Figure 1(a, b), but for the "ij-1" grid to the south of Mt. Cimone (left
 3 column) and the "i-1j-1" grid to the southwest of Mt. Cimone (right column), respectively.

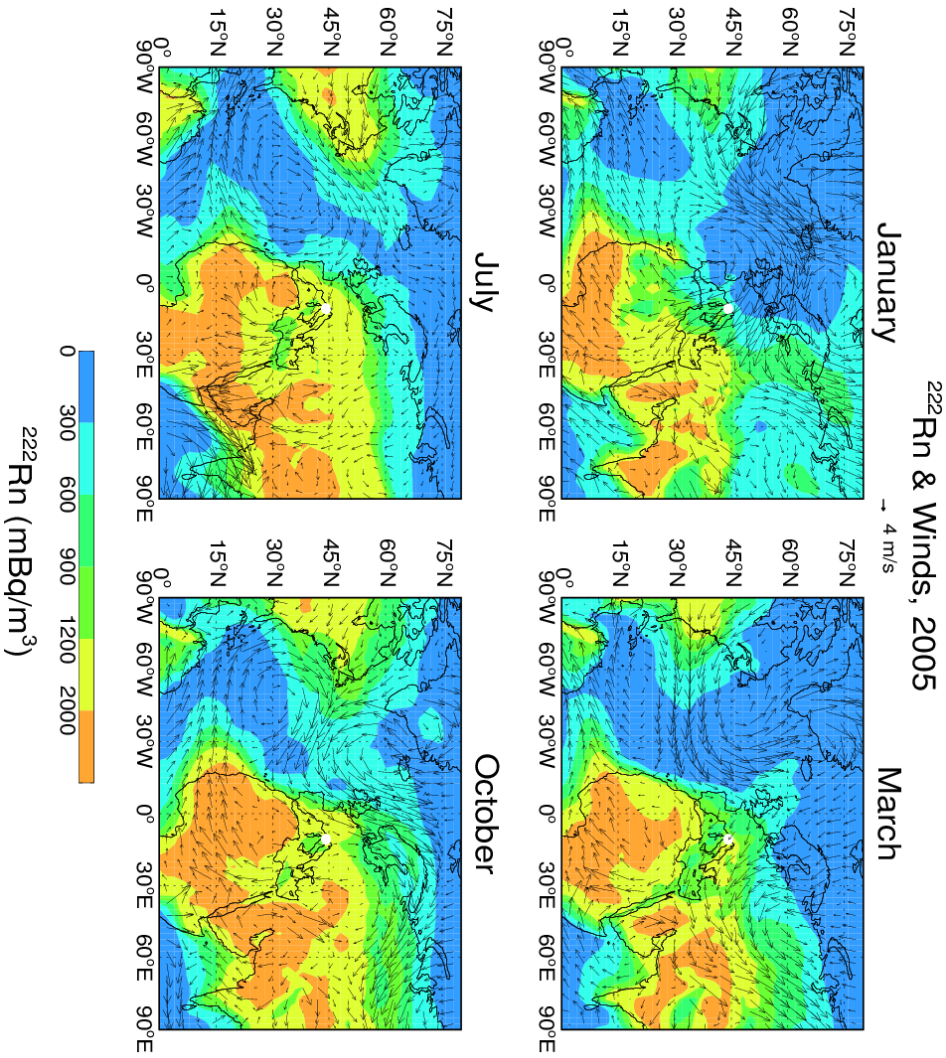
4

5

1
2
3
4
5
6
7
8
9
10
11
12
13
14
15



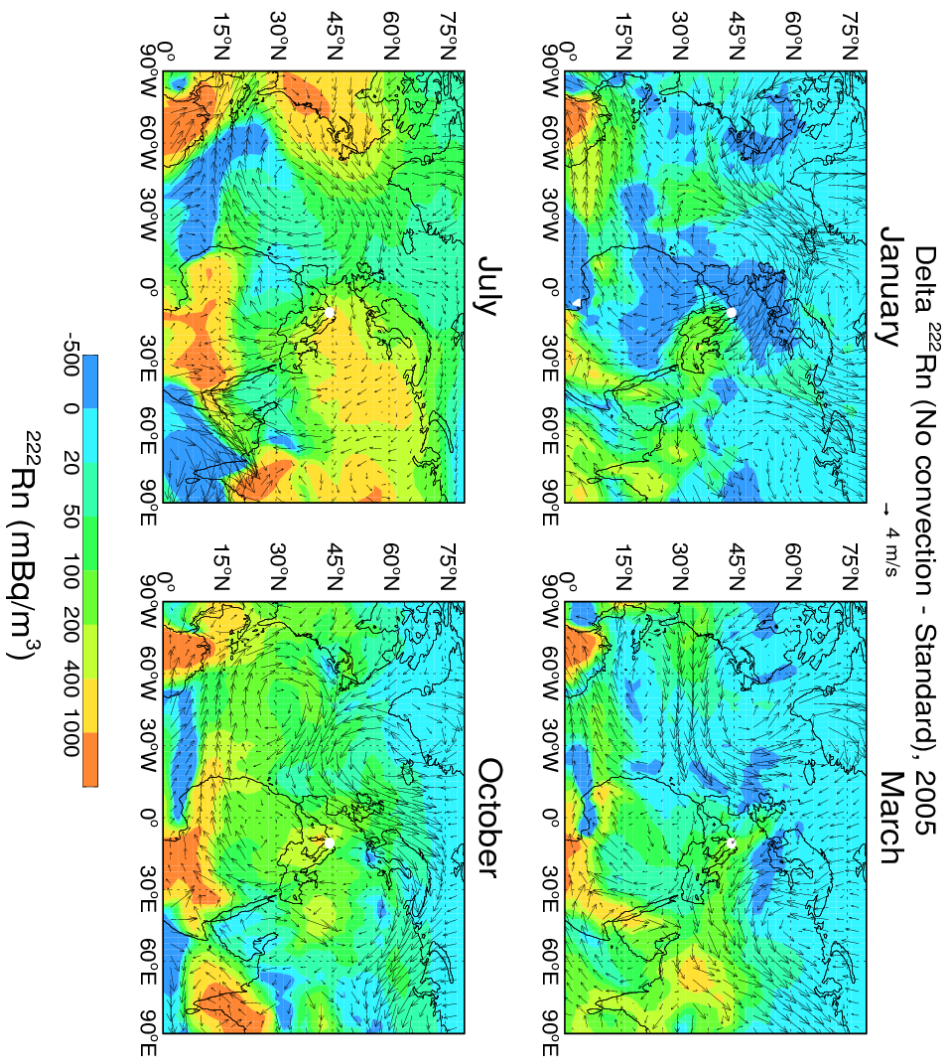
16 **SI Figure 3.** Comparison of GMI simulated monthly percentage fluctuations of ^{210}Pb and ^7Be
17 at Mt. Cimone (“ij-1” grid) between the standard (black dotted line) and the sensitivity runs.
18 The sensitivity runs are those without convective transport/scavenging (red dotted line),
19 without dry deposition (blue dotted line), and without scavenging (orange dotted line). The
20 observations are shown as green solid line.



1

2

3 **SI Figure 4.** Simulated monthly mean ^{222}Rn concentrations, at the elevation of Mt. Cimone.
 4 Arrows represent the seasonality of winds in the MERRA meteorological data. The white dot
 5 indicates the location of Mt. Cimone (44°12' N, 10°42' E, 2165 m asl).



1

2

3 **SI Figure 5.** GMI simulated differences of ²²²Rn concentrations at the elevation of Mt. Cimone
 4 between a sensitivity run without convection and the standard run. Arrows denote MERRA
 5 winds. The white dot indicates the location of Mt. Cimone (44°12' N, 10°42' E, 2165 m asl).